

AD-A058 960

AIR FORCE GEOPHYSICS LAB HANSCOM AFB MASS
DEVELOPMENT OF A CORONA ANEMOMETER FOR MEASUREMENT OF STRATOSPHERE--ETC(U)
MAR 78 R E GOOD, J H BROWN, G HARPELL

F/G 4/2

UNCLASSIFIED

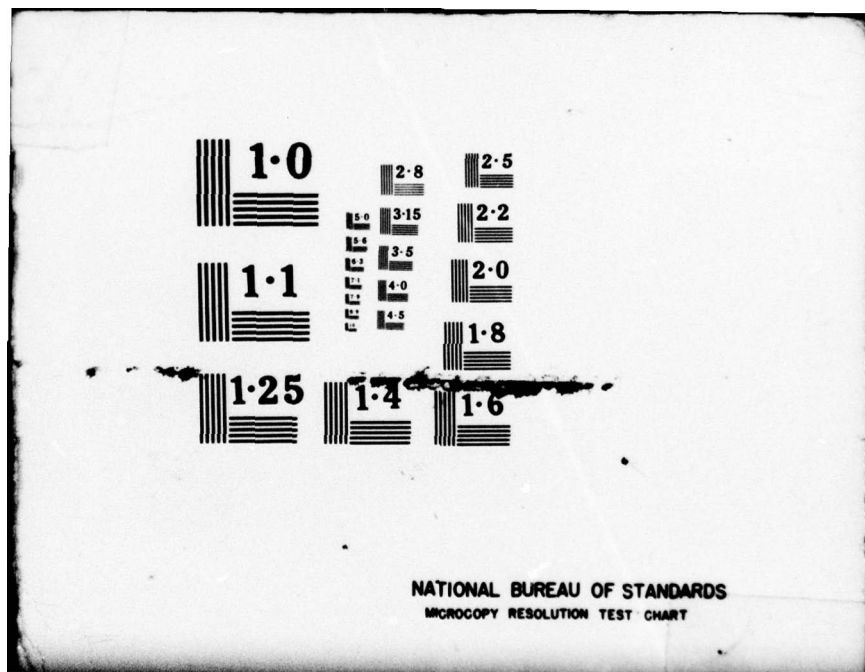
AFGL-TR-78-0070

NL

1 OF 1
ADA
058960



END
DATE
FILED
11-78
DDC

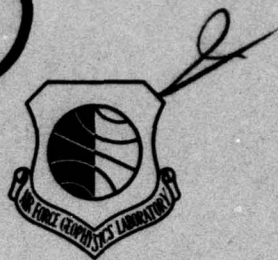


ADA058960

LEVEL II

AFGL-TR-78-0070
INSTRUMENTATION PAPERS, NO. 265

12

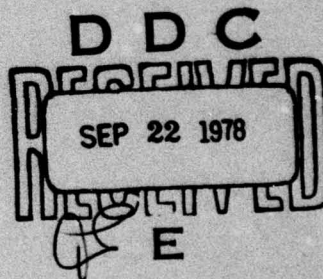


Development of a Corona Anemometer for Measurement of Stratospheric Turbulence

R. E. GOOD
J. H. BROWN
G. HARPELL

DDC FILE COPY

21 MARCH 1978



Approved for public release; distribution unlimited.

AERONOMY DIVISION PROJECT 6687
AIR FORCE GEOPHYSICS LABORATORY
HANSCOM AFB, MASSACHUSETTS 01731

AIR FORCE SYSTEMS COMMAND, USAF

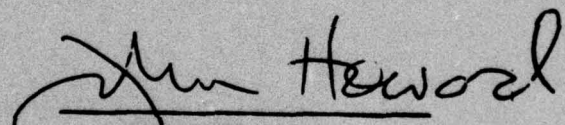


78 09 21 007

This report has been reviewed by the ESD Information Office (OI) and is releasable to the National Technical Information Service (NTIS).

This technical report has been reviewed and is approved for publication.

FOR THE COMMANDER



John Howard
Chief Scientist

Qualified requestors may obtain additional copies from the Defense Documentation Center. All others should apply to the National Technical Information Service.

Unclassified

SECURITY CLASSIFICATION OF THIS PAGE (When Data Entered)

REPORT DOCUMENTATION PAGE		READ INSTRUCTIONS BEFORE COMPLETING FORM
<p>14. SPONSORING SOURCE NUMBER AFGL-TR-78-0070, AFGL-IP-265</p> <p>6. TITLE (and subtitle) DEVELOPMENT OF A CORONA ANEMOMETER FOR MEASUREMENT OF STRATOSPHERIC TURBULENCE</p> <p>10. AUTHOR(S) R.E. Good J.H. Brown G. Harpell</p> <p>9. PERFORMING ORGANIZATION NAME AND ADDRESS Air Force Geophysics Laboratory (LKD) Hanscom AFB Massachusetts 01731</p> <p>11. CONTROLLING OFFICE NAME AND ADDRESS Air Force Geophysics Laboratory (LKD) Hanscom AFB Massachusetts 01731</p> <p>14. MONITORING AGENCY NAME & ADDRESS (if different from Controlling Office)</p>		3. FEDCEN'T'S CATALOG NUMBER
		5. TYPE OF REPORT & PERIOD COVERED Scientific. 9. Final rept.
		6. PERFORMING ORG. REPORT NUMBER IP No. 265
		8. CONTRACT OR GRANT NUMBER(S) 12 46p.
		10. PROGRAM ELEMENT, PROJECT, TASK AREA & WORK UNIT NUMBERS 62101F 66870501
		12. REPORT DATE 21 March 1978
		13. NUMBER OF PAGES 45
		15. SECURITY CLASS. (of this report) Unclassified
		15a. DECLASSIFICATION/DOWNGRADING SCHEDULE
16. DISTRIBUTION STATEMENT (of this Report) Approved for public release; distribution unlimited.		
17. DISTRIBUTION STATEMENT (of the abstract entered in Block 20, if different from Report)		
18. SUPPLEMENTARY NOTES		
19. KEY WORDS (Continue on reverse side if necessary and identify by block number) Stratosphere Turbulence Corona Anemometer		
<p>20. ABSTRACT (Continue on reverse side if necessary and identify by block number) The length of time pollution remains in the stratosphere depends upon the intensity of stratospheric turbulence. Measurement of stratospheric turbulence has been limited due to the lack of a suitable instrument. A new instrument has been developed to meet this need. The corona anemometer sensor development is described from the physical principles of operation through the electronic circuitry, laboratory and in-flight calibrations to the first test flight. The corona anemometer measures the stratospheric wind and turbulence by</p>		

DD FORM 1 JAN 73 1473 EDITION OF 1 NOV 65 IS OBSOLETE

Unclassified

SECURITY CLASSIFICATION OF THIS PAGE (When Data Entered)

409 578

Lee

Unclassified

SECURITY CLASSIFICATION OF THIS PAGE(When Data Entered)

20. Abstract (Continued)

detecting the amount of displacement the corona ion beam suffers in transversing a one inch gap exposed to the horizontal wind. The instrument response is linear and has a frequency response from 0 to 2000 Hz, sufficient to measure atmospheric turbulence directly. The use of this instrument in the measurement of stratospheric turbulence will significantly enhance the knowledge of stratosphere properties and improve the accuracy of environmental assessments.

Unclassified

SECURITY CLASSIFICATION OF THIS PAGE(When Data Entered)

ACCESSION for	
WRS	White Section <input checked="" type="checkbox"/>
DRG	Buff Section <input type="checkbox"/>
UNANNOUNCED	<input type="checkbox"/>
JUSTIFICATION.....	
BY.....	
DISTRIBUTION/AVAILABILITY CODES	
DRG	AVAIL. and/or SPECIAL
A	

Contents

1. INTRODUCTION	5
2. DEVELOPMENT OF CORONA SENSOR	6
2.1 Theory of Operation	7
2.1.1 Ion Generation	13
2.2 Engineering Design	15
2.2.1 Electronics Design	17
2.3 Calibration	19
2.3.1 Wind Tunnel Investigation of Corona Sensor	25
3. INITIAL FLIGHT TEST	38
4. CONCLUSIONS	43
REFERENCES	44

Illustrations

1. Stratospheric Corona Anemometer Schematic	6
2. Corona Target Plates	10
3a. Change in Corona Beam Area as a Function of Beam Displacement	11
3b. Linearity Test of Corona Beam Displacement	11
4. Corona High Voltage Dependence on Pressure	14
5. Flight Ready Photograph of Corona Anemometer	17

Illustrations

6. Electronic Block Diagram of Corona Anemometer	18
7. Electronic Circuit Flow Diagram	21
8. Bell Jar Velocity Calibration System	23
9. Air Velocity as a Function of Bell Jar Blower RPM and Air Pressure	23
10. Anemometer Voltage Calibration as a Function of Airstream Velocity	24
11. Strouhal Velocity Calibration	26
12. Power Spectral Density of Corona Anemometer Voltage Showing the Strouhal Frequency	27
13. Comparison of Bell Jar Velocity Calibration With In-flight Calibration Using Strouhal Velocity Calibration	27
14. Altitude Domain Useful for Strouhal Velocity Calibration	28
15. Wind Tunnel Calibration of Corona Anemometer	29
16. Power Spectral Density Comparison of Hot Wire and Corona Anemometer, $U = 10.91 \text{ m/sec}$, $X = 4.57 \text{ m}$	30
17. Power Spectral Density Comparison of Hot Wire and Corona Anemometer, $U = 10.6 \text{ m/sec}$, $X = 2 \text{ m}$	31
18. Power Spectral Density Comparison of Hot Wire and Corona Anemometer, $U = 2.8 \text{ m/sec}$, $X = 4.57$	32
19. Power Spectral Density Comparison of Hot Wire and Corona Anemometer, $U = 1.6 \text{ m/sec}$, $X = 4.57$	33
20. Power Spectral Density Comparison of Hot Wire and Corona Anemometer, $U = 3.14 \text{ m/sec}$, Grid Out	34
21. Summary of Power Spectral Density Distributions With Varying Levels of Turbulence	35
22. Velocity Acceleration Produced Inside the Anemometer	36
23. Turbulent Intensity Distribution Inside the First and Second Models of Corona Anemometer	37
24. Velocity Distribution Inside the First and Second Models of Corona Anemometer	37
25. Wind Tunnel Calibration of Velocity Including Effects of Angle of Attack	38
26. Altitude Profile of Initial Flight Test of Corona Anemometer	39
27. Observed Atmospheric Pressure and Temperature and the Velocity Measured by the Corona Anemometer	39
28. Velocity Variance Observed During Flight	41
29. Change of Power Spectral Density as Corona Instrument Passes Across a Turbulent Layer	42
30. Altitude Profile of Turbulent Dissipation Rate	43

Development of a Corona Anemometer for Measurement of Stratospheric Turbulence

1. INTRODUCTION

Man has the potential for discharging pollutants into the stratosphere that alters its chemical balance and results in serious environmental harm to the earth's climate and living organisms. This threat has been recognized and national efforts are underway to determine what harmful effects can be generated by the release of chlorofluoromethanes, principally from aerosols, release of NO_x in aircraft and missile exhausts and other sources of NO_x and halocarbons. The steps leading to an assessment of these potentially harmful sources involve careful examination of stratospheric composition and development of simulation models of the chemical and transport processes.

Turbulence is an important parameter describing the mixing of gases in the stratosphere. How rapidly a polluting gas mixes and is transported vertically indicates how long the pollution remains in the stratosphere. This residence time is key to predicting the harmful effect a particular pollutant will have. Estimates of one to two years residence time is one reason why very small concentration levels of pollution can produce significant changes in the stratospheric composition. At the present, no detailed picture exists that represents the actual physical processes, including turbulence, circulation, and winds, existing in the stratosphere. This has been due to lack of realization in earlier years that the stratospheric environment

(Received for publication 17 March 1978)

could be altered and result in serious changes in man's world. Until recently there have been too few measurements conducted to determine the transport processes. One inhibition to measurements has been the absence of satisfactory measurement techniques for stratospheric turbulence. This report describes the development and testing of a corona anemometer adapted to measure the stratospheric turbulence processes.

2. DEVELOPMENT OF CORONA SENSOR

The corona anemometer for detection of turbulence (CADT) measures wind velocity and turbulence by sensing the displacement fluctuation of ion current on a target. The CADT sensor consists of a corona source generating a flow of ions from the corona plate to the target plate. This is illustrated for one-dimension in Figure 1. The ions are generated in the electric field created between the high voltage applied to a fine point needle and the voltage applied to the corona control plate. A small hole in the control plate, $1/4$ in. diameter, on the centerline of the needle allows a fraction of the corona current ≈ 10 percent to be drawn to the target plate. The target plate is segmented into halves at each side of the centerline. The ion stream diffuses outward as it transverses the air gap between the two plates. In the absence of a wind, the current collected by each half of the target plate is identical. With a wind blowing between the two plates, the ions are deflected downstream by the wind. The difference in current collected on the two plates is a measure of the wind speed.

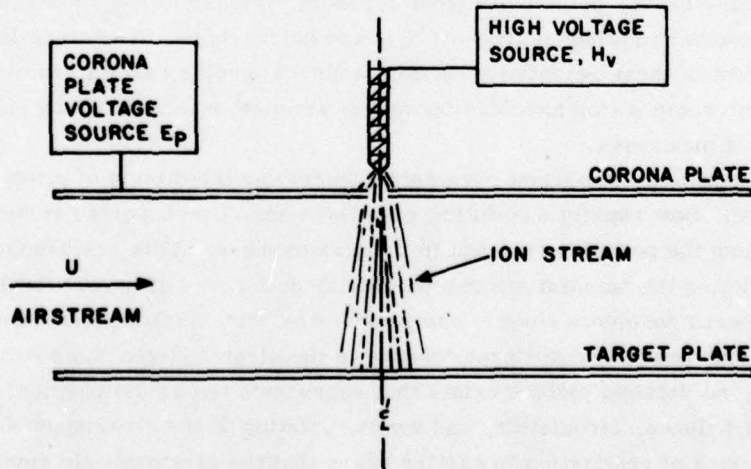


Figure 1. Stratospheric Corona Anemometer Schematic

The advantage of CADT for stratospheric wind measurement is the ease by which the sensor response to windspeed can be maintained uniform, while the force of the wind dramatically changes with altitude due to the varying atmospheric density. Mechanical anemometers, in contrast, are optimized to a particular density altitude.

Measurement of stratospheric turbulence is very difficult. The stratosphere, in contrast to the troposphere, has a low density and consequently low levels of turbulent energy. This means that the usual turbulence detectors employed in the troposphere are inadequate. Mechanical anemometers have too much inertia, the energy threshold of acoustic detectors is too high, and instrumental errors dominate the output of hot wire detectors. Optical anemometers require a large density of light scattering particles which are not found in sufficient density in the stratosphere. A new type of turbulence detector was needed for the stratosphere.

A suitable anemometer is one based on measuring the advective motion of ions traversing between two opposed plates. The ions can be produced by a stable or corona with electrical control of the corona current to maintain a uniform flow of ions. The corona anemometer has been used to study turbulence in wind tunnels¹ and was first applied for stratospheric turbulence measurement by Barat.² A corona anemometer to measure gas flow rates was successfully developed by Lilienfeld³ for use on stratospheric particle samples. This report describes the development of a corona anemometer, its calibration, and the results of the initial stratospheric turbulence measurements.

2.1 Theory of Operation

A corona is an electrical breakdown of a gas which occurs where nonuniform electric fields are encountered. It can occur with asymmetrical electrode geometries such as point to plane, sphere to cylinder, or wherever sharp edged or small radii electrodes appear. Breakdown is initiated by the high fields concentrated at one or both of the electrodes but complete breakdown to an arc, at or near the corona threshold, is precluded by the weak field between the electrodes. The appearance of corona current at the threshold levels is usually unstable due to an insufficient number of triggering electrons. Above threshold and at a current on the order of microamperes, steady corona is achieved. Here an increase in current

1. Franzen, B., Fucks, W., and Schmitz, G. (1961) Corona anemometer for measurement of turbulence components, Zeit. für Flugwissenschaften 9:347-351.
2. Barat, J. (1975) Une méthode de mesure directe du taux de dissipation d'énergie turbulente dans la stratosphère. Compt. Rend. Acad. Sci. Paris B281: 53-56.
3. Lilienfeld, Pedro, Solon, L., and DiGiovanni, Hugo (1967) Ion tracer anemometer for the measurement of low density flows. Rev. Sci. Inst. 38:405-409.

is nearly proportional to a potential increase. This is the so-called Ohm's Law Regime in which the CADT sensors operate most frequently. Beyond this region, current increases parabolically with potential and eventually results in a complete transient arc or spark breakdown. Tests performed with CADT sensors reveal that steady corona onset is achieved at tens of volts above threshold and spark breakdown occurs at a few hundred volts above onset. Actual values depend upon pressure P , and electrode separation, t . Threshold voltages follow the well known Paschen Law where $V_B = V_B(Pt)$.

The basic theory of operation of the corona anemometer can be predicted from the corona theories developed by Loeb,^{4,5} Brown,⁶ and McDaniel and Mason.⁷ Corona anemometers have been developed to measure turbulence in wind tunnels¹ and to measure surface winds.⁸ A new development was required to adapt the corona sensor to measure stratospheric winds relative to the motion of a floating balloon and to directly detect the existence of turbulence and measure the turbulent intensity.

Conceptually, the displacement of the ions can be seen as the result of the interaction of the ion stream and airstream. The displacement angle, θ , is defined by the normal displacement length D , of the ion stream from the centerline and by the path length L over which the ions drift to the target. For small deflections, conservation of linear momentum requires that the tangent of θ be equal to the ratio of the initial momenta of the airstream to ion stream. This is represented as:

$$\tan \theta = \frac{D}{L} = \frac{(mU)_{\text{air}}}{(mv_d)_{\text{ions}}} \quad (1)$$

where m is the mass of air or ions which interact within the ion stream volume V ; U is the freestream air velocity, and v_d is the ion drift velocity.

To a first approximation the momentum, mU , can be related to the mass flow (ρUA) by accounting for the interaction volume V and the respective cross sectional area of interaction, A , where:

4. Loeb, L. B. (1960) Basic Processes of Gaseous Electronics, Univ. of California Press, Los Angeles.
5. Loeb, L. B. (1965) Electrical Coronas, Univ. of California Press, Los Angeles.
6. Brown, S. C. (1966) Introduction to Electrical Discharges in Gases, John Wiley & Sons, New York.
7. McDaniel, E. W., and Mason, E. A. (1973) The Mobility and Diffusion of Ions in Gases, John Wiley & Sons, New York.
8. Waletzko, J. A. (1975) A new ion displacement system to measure the two dimensional wind vector, Tech. Conf. on Automated Meteorological Systems, Washington, D.C.

$$mU = (\rho UA) \times \frac{V}{A} \quad (2)$$

It follows that,

$$\frac{D}{L} = \frac{(\rho UA)_{air} \times V/A_{air}}{(\rho_i v_d A)_{ions} \times V/A_T} \quad (3)$$

where A_T is the area of the target upon which the ions impinge. Experiments have shown that by maintaining the potential difference E_p constant between control plate and target, A_T is a weak function of ρ . Also the total current collected, I_T , is proportional to the ion mass flow, $I_T \propto (\rho v_d A_T)_{ions}$. This results in the ability to measure mass flux of the airstream as:

$$\rho u = C_1 D I_T$$

where C_1 is a constant containing the physical parameters of the sensor.

The details of operation in terms of ion mobility and corona current voltage relationships, have been described by Waletzko.⁸ The corona ions acquire a drift velocity parallel to the electric field across the two plates as

$$v_d = \mu \cdot E \quad (4)$$

where μ is the ion mobility and E is the electric field established by the potential difference between the two plates separated a distance L . This linear relation holds as long as $E/\rho < 2$ volt/cm torr and if E is uniform. The ion transit time between the two plates is therefore

$$\tau = \int_0^L \frac{dz}{\mu E} \approx \frac{L}{v_d} \quad (5)$$

The distance the ions are swept downstream during the transit time is

$$D = U_{air} \tau = U \int_0^L \frac{dz}{\mu E} \quad (6)$$

The ion mass and the air molecule mass are nearly identical so that the ions acquire a velocity component parallel to the wind due to momentum transfer. This velocity component is acquired in a time period of a few collisions ($t = 1-10$ nsec) which is small in comparison to the ion transit time.

The corona current is collected on an electrode consisting of a matrix of small resistors. The resistors are connected together in such a manner as to effectively measure the current falling on each of segment. Subsequent development and flight experience has shown the multi-element matrix to have insufficient velocity resolution due to the spacing between elements. A four plate electrode is currently being used with excellent results. Considering only one-dimension, the displacement of the ion beam is sensed by measuring the difference in current collected on the plates (see Figure 2). The corona current collected has been measured across the surface of a test electrode and found to have a Gaussian-shaped distribution with a half peak width of ≈ 5 mm. With this symmetric distribution, the difference in currents represents a displacement of the ion beam and can be visualized as a difference in beam area projected on each half of the electrode. For a uniform current distribution the area difference in terms of displacement, D , is:

$$\frac{A_2 - A_1}{A} = \frac{2 \sin^{-1} \left(\frac{D}{r} \right)}{\pi} + \frac{2}{\pi} \left(\frac{D}{r} \right) \sqrt{1 - \left(\frac{D}{r} \right)^2} \quad (7)$$

where r is the radius of the corona beam. This can be approximated using the following expression as shown in Figure 3a

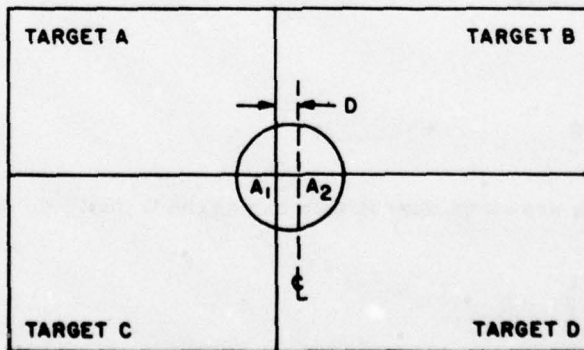


Figure 2. Corona Target Plates

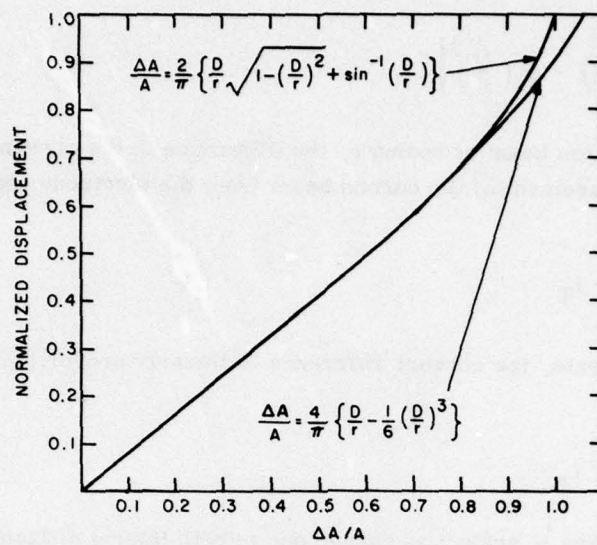


Figure 3a. Change in Corona Beam Area as a Function of Beam Displacement

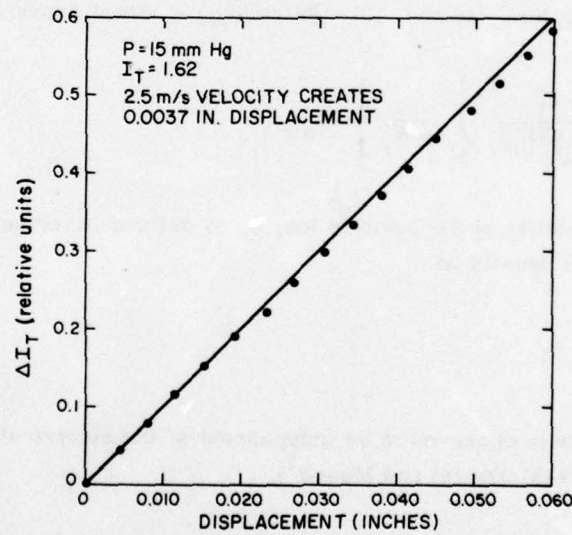


Figure 3b. Linearity Test of Corona Beam Displacement

$$\frac{A_2 - A_1}{A} = \frac{4}{\pi} \left\{ \left(\frac{D}{r} \right) - \frac{1}{6} \left(\frac{D}{r} \right)^3 \right\} \quad . \quad (8)$$

For a narrow corona ion beam of radius r , the difference in the currents is proportional to the displacement of the corona beam from the electrode center,

$$I_2 - I_1 = \frac{A_2 - A_1}{A} I_T \quad . \quad (9)$$

For small displacements, the current difference is linearly proportional to the displacement

$$I_2 - I_1 = \frac{4}{\pi} \left(\frac{D}{r} \right) I_T \quad . \quad (10)$$

The corona beam radius is subject to change due to both lateral diffusion and effects of the nonparallel electric field, that is, $r = L \cdot f(E_p)$. If only lateral diffusion existed, the beam radius function would be (McDaniel and Mason, 1973)

$$f_1(E_p) = 0.173 (E_p L)^{-1/2} \quad . \quad (11)$$

The expression relating wind velocity to a measurement of corona current can now be written. Combing Eqs. (6) and (10), the velocity-current expression is

$$I_2 - I_1 = \left[\frac{4}{\pi} \frac{I_T}{L f(E_p)} \int_0^L \frac{dz}{\mu E_p} \right] U_{air} \quad . \quad (12)$$

The ambient mobility of the positive ion, μ , is defined in terms of the reduced mobility, K_o and gas density as

$$\mu = K_o \left(\frac{\rho_o}{\rho} \right) \quad . \quad (13)$$

The reduced mobility is observed to be independent of the electrical field provided $E/p < 30$ (v/cm torr) (McDaniel and Mason⁷).

Thus the integral in Eq. (12) can be evaluated as

$$\int_0^L \frac{dz}{\mu E_p} = \frac{L \rho}{K_o \rho_o} \frac{g(Z)}{f(E_p)} \quad (14)$$

with the result of current difference given as

$$I_2 - I_1 = \frac{4 g(Z) \rho}{\pi K_o \rho_o} \frac{I_T}{E_p} \frac{U_{air}}{f(E_p)} \quad (15)$$

When the CADT was operated with fixed target current, I_T , the current difference was observed to be a function of ρU_{air} and having an $E_p^{3/2}$ dependence. This implies that $f(E_p) = \beta E_p^{1/2}$ and β is a proportionality constant as shown in Eq. (11)

$$I_2 - I_1 = \left(\frac{4 g(Z)}{\pi K_o \rho_o \beta E_p^{3/2}} \right) I_T \rho U_{air} \quad (16a)$$

The CADT can be operated at a fixed E_p field strength with a mass flow detection

$$\rho U = C \left(\frac{I_2 - I_1}{I_T} \right) \quad (16b)$$

where the constant $C = \frac{\pi K_o \rho_o E_p f(E_p)}{4 g(Z)}$ is determined by calibration. This is the basic velocity relation used to interpret measurements with the corona anemometer operated at fixed I_T and E_p .

2.1.1 ION GENERATION

The corona can be generated in many ways: sphere-to-cylinder, point-to-point or point-to-plate. In this instrument, the corona ions are created by high voltage breakdown between a fine needle point separated 3 mm from the hole in the upper plate. The gap distance between the needle tip and the hole is adjusted until a fixed, $2 \mu A$ current exists when 1700 volts is applied at 120 mm Hg pressure in a dry air atmosphere. The corona current generated can be expressed as

$$I_c = (V - V_g) v_d h \quad (17)$$

where V is the potential difference between the needle and plate, V_g the threshold voltage for creation of corona current (Geiger counter region) and h is a complex

geometric parameter defining the two electrodes. At the high field strength $E/p > 2$ V/cm-torr, the drift velocity follows the relation

$$v_d \propto K_o \sqrt{E_c/p} \quad . \quad (18)$$

The corona current relation when the applied voltage V is much greater than V_g is

$$I_c = (K_o h)(V - V_g) \sqrt{\frac{V}{\rho l}} \quad (19)$$

where l represents the separation of approximately 3 mm between the needle point and the plate. The corona instrument is operated to maintain a constant corona current throughout the flight. Thus it is necessary to lower the high voltage potential on the needle as the instrument ascends to higher altitudes. Laboratory measurements at constant temperature, shown in Figure 4, confirm the $\rho^{1/2}$ dependence of the corona current.

A small fraction of the corona current generated is drawn through the 6 mm hole in the upper plate, down to the collector plate. The fraction of current

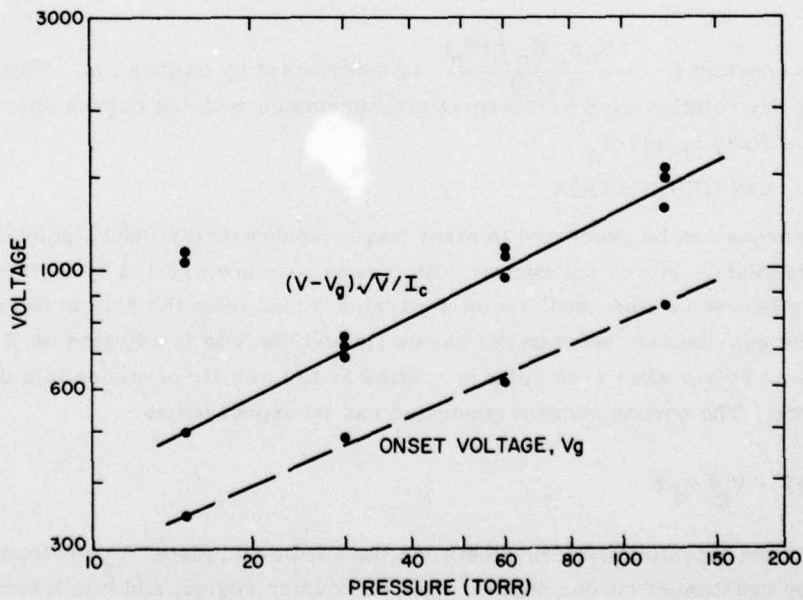


Figure 4. Corona High Voltage Dependence on Pressure

drawn (≈ 10 percent) depends upon the ion density in the cavity region and the field strength through the hole. The total current collected is referred to as the target current I_T . The current collected has a nonlinear dependence on E_p and a weak linear dependence on I_c . The total target current increases with pressure to a pressure between 5 and 20 mm (depending upon E_p), after which the target current decreases and eventually reaches zero.

Detailed observations reveal that the target current is independent of wind velocity at air densities below 2×10^{-5} g/cm³. At higher densities, the target current decreases with increasing velocity. This decrease in current is believed to occur in the neighborhood of the upper plate hole where a portion of the current is blown to the upper plate by air passing up into the cavity.

2.2 Engineering Design

Engineering development of the sensor components required evaluation and optimization of both the electrical performance and aerodynamic performance. Wind tunnel testing was used to evaluate the aerodynamic performance (see section 2.4) and select an optimized geometry. The first parameter to be chosen was the plate separation distance L . A 2.5 cm (1") separation was chosen as a compromise between sensitivity, smooth airflow and minimization of spread of the corona ion beam across the gap. A large radius of curvature at the edges of the plate was found to be necessary to prevent separation of flow at the edges which would lead to internally generated turbulence. The stand-off rods holding the top plate to the sensor were found to be useful as a means of calibrating the flow. The wake behind the rods, under certain Reynolds number conditions, has regularly spaced eddies which produce a single frequency as they are carried across the corona beam at the speed of the airstream. The airstream velocity can be measured by observing the frequency of arrival of the turbulent eddies.

Fabrication and shaping of the high voltage probes was a key factor in the successful development of CADT. The high voltage probe must have a sharp point to achieve steady operation of a corona at voltages considerably below spark breakdown voltages and to minimize the probe heating. Heat conduction from the point itself to a heat sink is vital in order to preserve the integrity of the sharpened probe and achieve 20-30 hour operational lifetimes. The composition of the needle, therefore, must be such that the probe has rigidity, is machinable and has good conductivity. Numerous materials were tried and rejected before finding the best material. Tool steel (sewing machine needles) had poor conductivity and the points rapidly melted. Tungsten carbide was too hard to form an adequate point. Gold and platinum did not last long. A needle formed from 90 percent platinum and 10 percent Iridium was found to hold a good point in excess of 20 hr of operation.

The best design was found using a 3 mm long, 0.6 mm diameter needle with a 20 degree taper to a tip diameter of 0.08 mm. The needle was found to survive the occasional arc-overs that occurred during various tests. An excessive number of hours of operation, however, results in a ball forming on the tip of the needle.

The high voltage probe is mounted in a tapered holder. The taper \approx 60 degree included angle is required to achieve the best heat conduction by getting the copper holder as close to the probe point without producing arc-over. The needle is initially polished to a fine tapered (\approx 20 degree angle) point. The CADT is operated for two hours to achieve a "burn in" of the probe point. Initially, the high voltage required for corona is about 10 percent lower than the final operating level. The probe point during the first hours of operation undergoes melting, and melts back to a small radius point \approx 0.1 mm, requiring a slightly higher voltage for corona. Thereafter, the voltage remains constant. The anticipated velocities range between 0 and 20 m/sec with a resolution requirement of 1 cm/sec. The velocity range that can be measured is a function of the ion drift velocity. This is determined by the choice of the plate voltage, E_p . A high E_p implies a fast drift velocity and a small deflection for a given airstream velocity. A constant E_p of 350 volts was found to give the desired resolution and operate the corona in the desired linear range over the expected velocity range. (The plate voltage is correctly $E_p \cdot L$.)

The CADT operates within two constraints. Too high an operation potential creates a strong field between the needle and top plate, reduces the current I_T that can be pulled to the collector plate. Decreasing the applied potential increases the collected current until the applied potential approaches the corona threshold potential, a point where no corona will occur. Thus operating the high voltage (HV) to produce the fixed 2 μ A of corona current, requires dropping the E_p at pressures below 15 mm Hg to 100 volts in order to be above the threshold potential. This increases the velocity sensitivity, that is, a given velocity requires a larger $\Delta I/I_T$ for a smaller E_p . This limits the maximum velocity that can be detected before $\Delta I/I_T$ approaches unity. Subsequent flight experience has shown the velocities to be lower at the high altitude so that dropping E_p is not expected to cause problems.

The high corona voltage, $E_c t$, required to produce the desired constant corona current, I_c , varies with the atmospheric density as shown by Eq. (19) and measured in Figure 4. A circuit was designed to vary the high voltage as required to achieve a constant corona current of two μ A with a 12 sec response time. The high voltage ranges from 1700 volts at 120 mm Hg to 700 volts at 15 mm Hg pressure. The electric field between the two plates is perturbed by the high voltage which creates a small nonlinear variation in velocity response with altitude. Calibration of the CADT is required over the anticipated operating region. Heads have been assembled from identical components in a very precise manner. Variations in

performance between "identical" units usually can be traced to some slight misalignment that can be corrected.

The output of the CADT sensor is measured on each axis. Four data channels are required to measure the high and low gain outputs of the x and y axis with the high gain output ten times the low gain. These channels measure primarily the mean windspeed. The turbulence is measured with four data channels having a high pass filter removing signals below 20 Hz. There are four ac channels, amplified a factor ten over the dc channels, which measure the velocity fluctuations between 20 Hz and 2000 Hz.

The developed sensor is shown in Figure 5. A total of four sensors were built, with the best two flown in the initial flight test, described in Section 3.

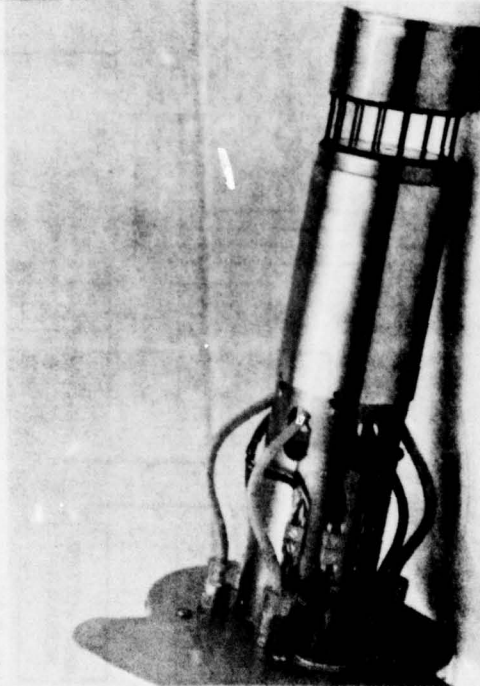


Figure 5. Flight Ready Photograph of Corona Anemometer

2.2.1 ELECTRONICS DESIGN

The current from each target A, B, C, and D goes to the preamp (see Figure 6) where it is converted to a voltage, through the preamp, and to the output, where the output is low impedance. The preamp also sums all of the current that is collected on the four targets and this is called E_{TT} and is measured as a voltage across a resistor. To measure a signal in the +x direction, the x amplifier adds the voltages as A + B and C + D, then subtracts the sum of (C + D) from (A + B). This

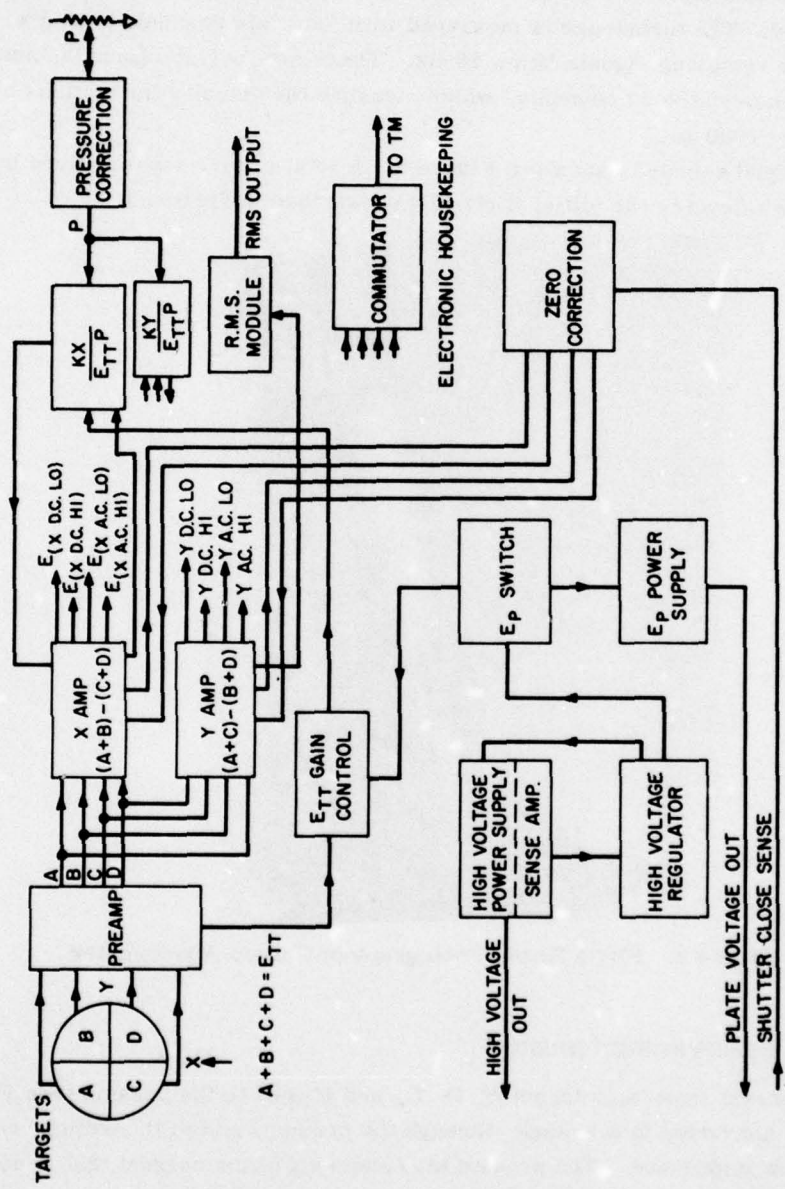


Figure 6. Electronic Block Diagram of Corona Anemometer

latter signal (E_x) is then sent to a function card where it is divided by the product of E_{TT} and a voltage proportional to the ambient pressure. The pressure correction circuit corrects for the offset and scale factor of the pressure transducer and produces a linear voltage output. The signal $E_x/(E_{TT} \cdot p)$ is then sent back to the amplifier where various gained outputs are produced. The dc output is actually the signal with only a high frequency cut off, the ac outputs goes through an additional low pass filter leaving 10 Hz to 1 KHz with a 3 db roll off on the high end.

From the y amplifier, the output is fed to an RMS module and the RMS value is then transmitted.

A zero correction circuit is used to correct for two errors, one being the long time drift of the amplifiers and the more important reason being the change in beam pattern with time due to wear of the point. When the shutter is closed, a cylindrical shell encloses the sensing head air gap. A check is made of the output of the dc low gain amplifier. If it is not at zero, a digital counter generates a voltage output until the output amplifier is zero. At that point, it stops counting and holds this offset until it is called for again.

The corona current, the current from point to control plate, is maintained at $2 \mu\text{A} \pm 0.03$ for all pressures. The corona current goes through an isolation amplifier, the output of the amplifier is a linear function of current and this is fed to an electronic servo High Voltage Regulator. The output is fed to a dc to dc high voltage power supply and maintains constant current. The high voltage control is the voltage from the high voltage regulator and this is a function of pressure. This control voltage is used to switch E_p from 350V at relatively high pressures to 100V at low pressures. When we shift the E_p voltage, we also change the gain of the E_{TT} gain control. The commutator is a multiplexer used to sample all of the different functions necessary to determine if the system is operational. These sampled voltages would be the output of $B+$ and $B-$ regulators, battery voltages, shutter position open or closed, main boom position, and other housekeeping data. Figure 7 shows the electronic block drawing in greater detail.

2.3 Calibration

The CADT system was calibrated for velocity using two approaches. The first calibration was conducted inside a 45 cm (18 in.) laboratory bell jar using a small turbine air blower to generate the velocity through the sensor. The second calibration was performed at the Wright Brothers Low Speed Wind Tunnel at MIT.

The bell jar calibration was set up as shown in Figure 8. The flow velocity inside the duct was measured using a Pitot tube and Baratron absolute and differential pressure sensors. The velocity calibration is given in Figure 9. The CADT system velocity calibration in terms of voltage output V_x or V_y is presented in

Figure 10. Separate calibrations for each sensor and the X and Y directions are required but they are similar in response. The velocity in each axis, U_x and U_y , is determined to be functions of the measured voltage in each axis.

$$\left. \begin{array}{l} U_x = V_x \\ U_y = V_y \end{array} \right\} \text{Low gain}$$

$$\left. \begin{array}{l} U_x = V_x/10 \\ U_y = V_y/10 \end{array} \right\} \text{High gain}$$
(20)

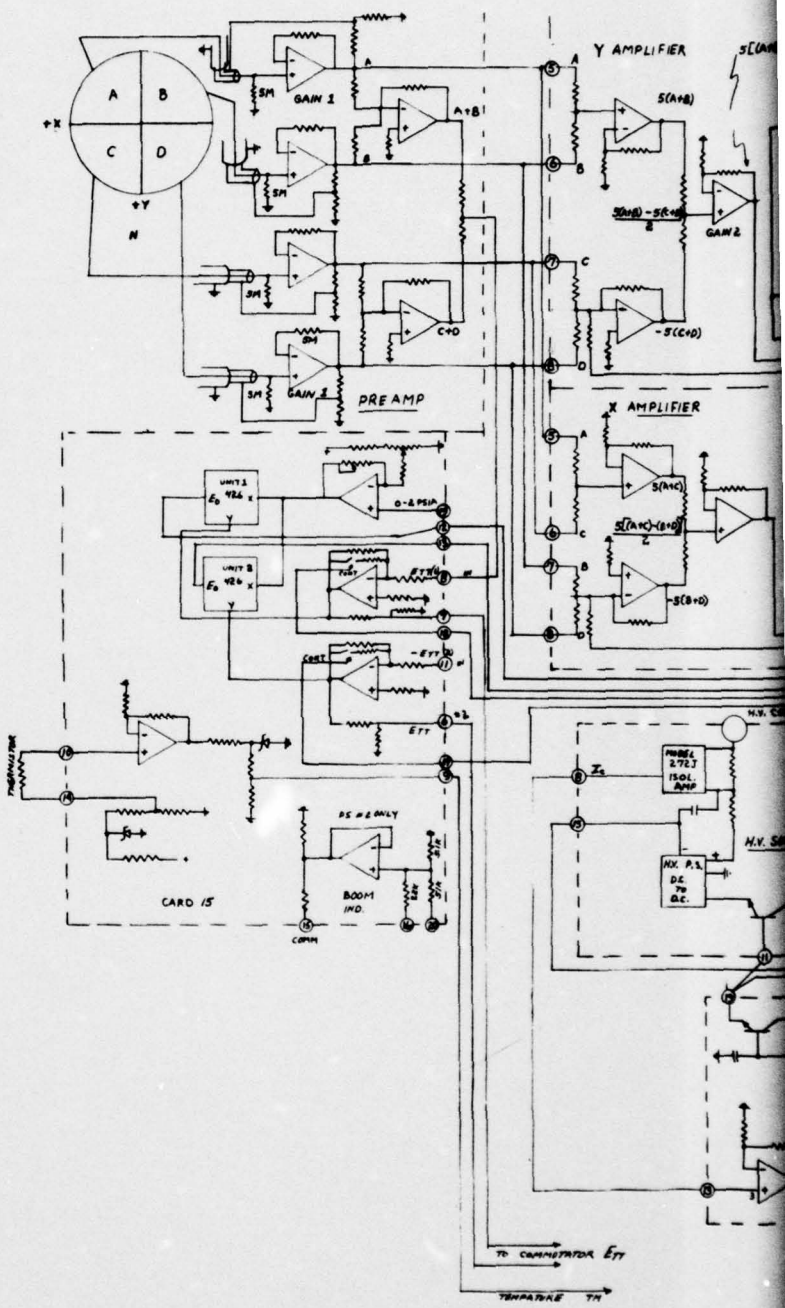
The velocity calibration could not be accurately conducted at speeds less than 0.5 m/sec at low pressures due to the lack of an accurate and independent velocity standard. A test of the linearity of the velocity response was developed and it demonstrated the CADT has excellent linear velocity response. Thus the calibration consists of performing an accurate measurement over one velocity range and establishing the existence of a linear response over the entire velocity range. The linearity was proven using a special plate that permitted translating the collector plate along the velocity vector in steps as small as 0.001 in. The procedure was to establish a given velocity and measure the deflection, $\Delta I/I_T$. The flow was turned off and the collector plate translated relative to the needle until the same $\Delta I/I_T$ was observed. The flow is then turned on and the deflection $2 \Delta I/I_T$ is measured. The flow is then turned off and the collector plate translated. This was repeated in increments out to a $\Delta I/I = 0.33$ as shown in Figure 3b.

A calibration in flight can be obtained by taking advantage of the existence of vortex shedding from the standoffs separating the two plates. A regular spaced Karman vortex street is generated as the uniform flow separates passing around the circular cylinder standoffs separating the two plates. The shedding frequency, n , of the individual vortexes can be made dimensionless in terms of the cylinder diameter, D , and the flow velocity, U , as

$$S = \frac{nD}{U} \quad (21)$$

where S is shown as the Strouhal number. The vortex is observed to depend on the flow Reynolds number. The vortex street is stable and regular only between Reynolds No. 40 and 150 (Roshko,⁹ Webster,¹⁰ and Tritton,¹¹). The vortex street

9. Roshko, R. (1954) On the Development of Turbulent Wakes From Vortex Streets, NACA Rep 1191.
10. Webster, C.A.G. (1964) An experimental study of turbulence in a density-stratified shear flow, *Fluid Mech.* 19:221-245.
11. Tritton, D.J. (1970) Experiments on the Flow Past a Circular Cylinder at Low Reynolds Numbers.



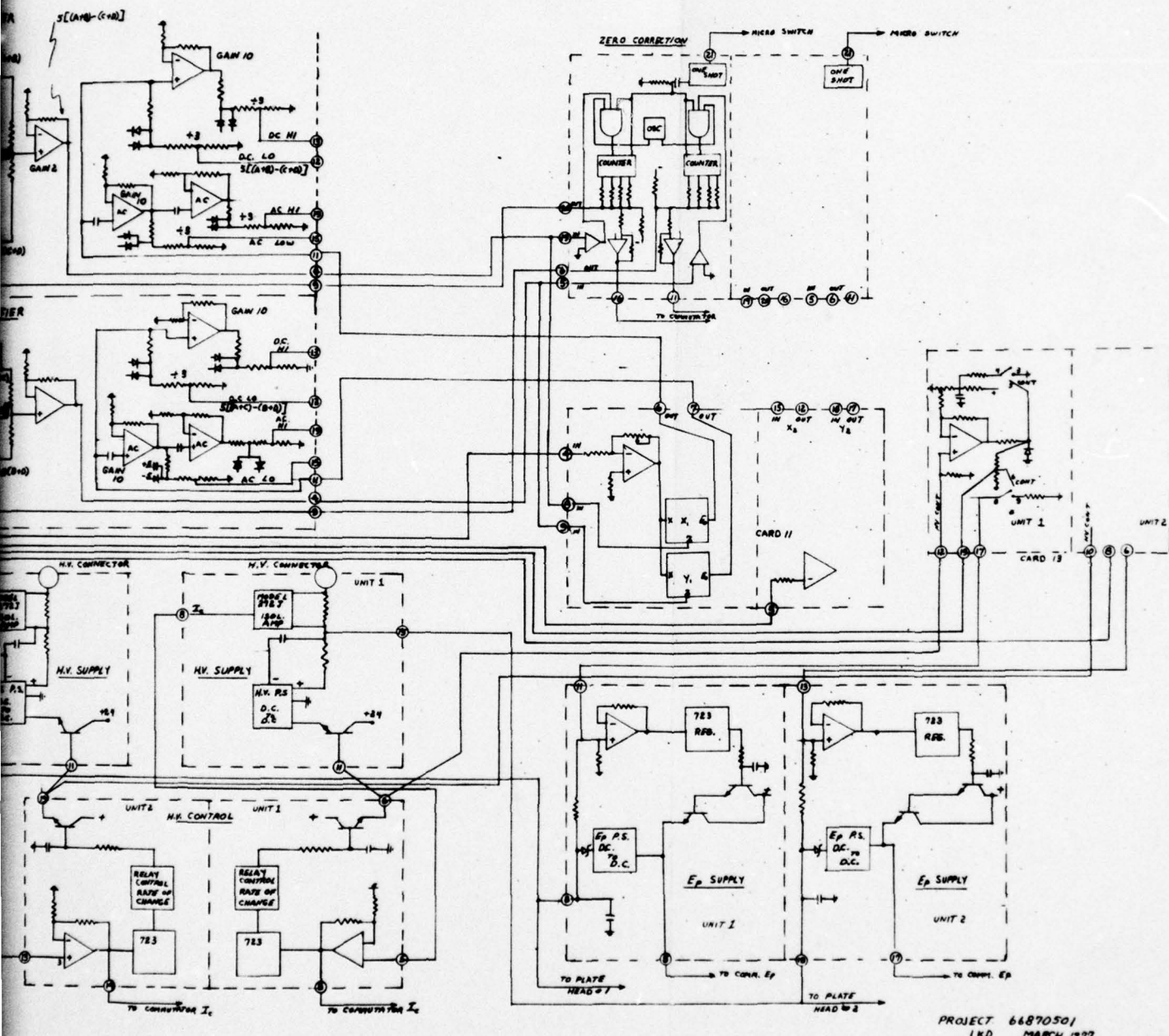


Figure 7. Electronic Circuit Flow Diagram

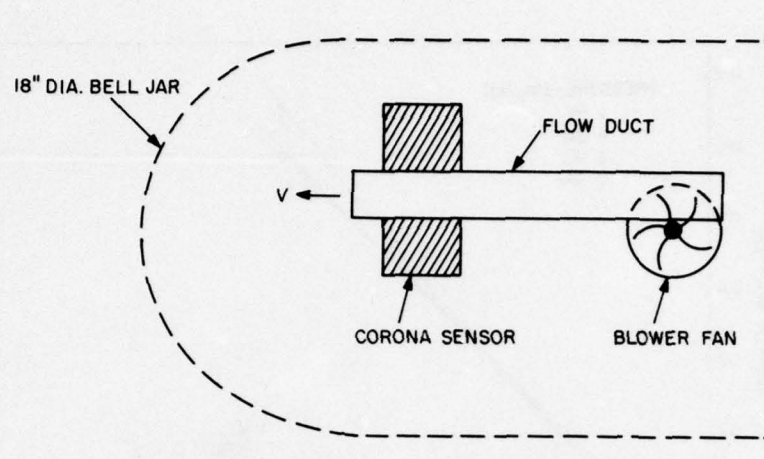


Figure 8. Bell Jar Velocity Calibration System

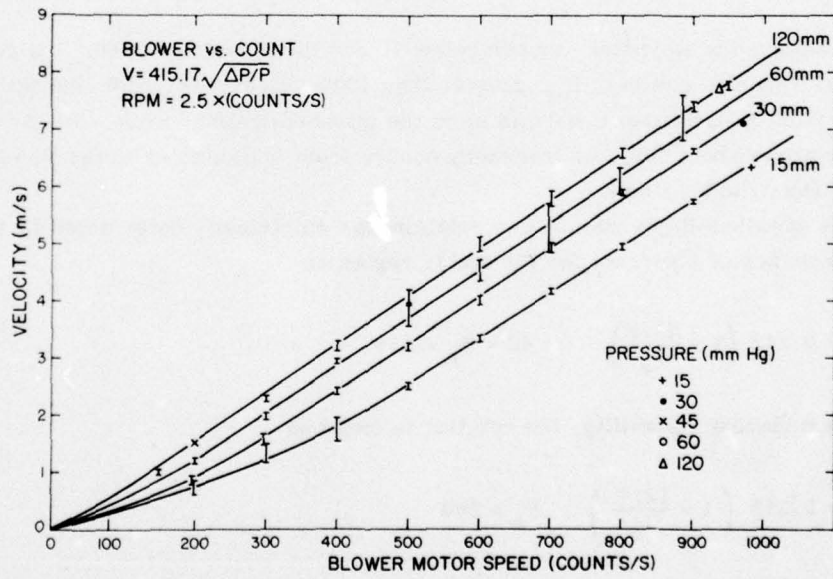


Figure 9. Air Velocity as a Function of Bell Jar Blower RPM and Air Pressure

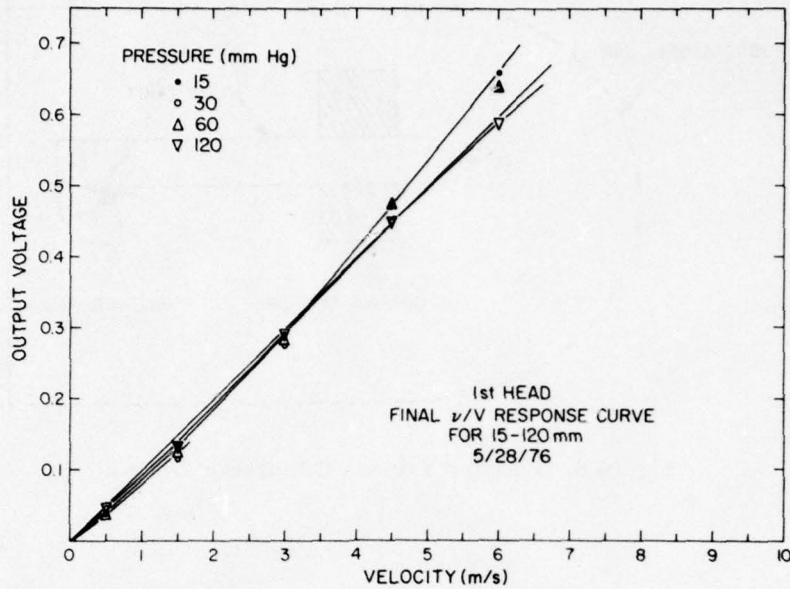


Figure 10. Anemometer Voltage Calibration as a Function of Airstream Velocity

is not observed at Reynolds number below 40 and the Strouhal number is a constant 0.212 at Reynolds number, R_e , greater than 1000. Below $R_e = 150$, the frequency occurs from instabilities that build up in the attached laminar wake. At Reynolds number above about 300, the frequency occurs from instabilities in the flow separation off the cylinder itself.

The Strouhal-Reynolds number relation was empirically determined by Roshko⁹ to an accuracy of 1 percent for the stable region as

$$S = 0.212 \left(1 - \frac{21.2}{R_e} \right) \quad 40 < R_e < 150 \quad (22)$$

For the turbulent instability, the relation is found as

$$S = 0.212 \left(1 - \frac{12.7}{R_e} \right) \quad R_e > 300 \quad (23)$$

The transition to turbulent flow separation occurs earlier in the presence of turbulent flow when the velocity fluctuations exceed 0.1 percent (Webster¹⁰).

The flow velocity as a function of Strouhal frequency can be determined from Eqs. (21) and (22) using the definition of Reynolds number and expressed as

$$U_{(\text{cm/s})} = \frac{nD}{0.212} + \frac{21.2}{D} \nu \quad (24)$$

where ν is the kinematic viscosity. This relationship is plotted in Figure 11 for various values of viscosity.

The CADT instrument ac signal is frequency analyzed to evaluate the power spectrum. A typical spectrum is shown in Figure 12.

The flight data was sampled and comparison between the velocity determined from the Strouhal frequency using Eq. (24) and the velocity determined from the corona displacement using Eq. (16). The results are shown in Figure 13. Excellent agreement is found between the two velocities. Note, the Strouhal velocity is resolved into x and y coordinates for comparison purposes using the angle of the flow determined by the corona sensor. The velocity range that can be calibrated with the Strouhal frequency at a given altitude is shown in Figure 14.

2.3.1 WIND TUNNEL INVESTIGATION OF CORONA SENSOR

An instrument to be placed in a moving airstream should be carefully studied to examine what perturbations are created in the flow by the instrument itself. Ideally, the aerodynamic investigations should be conducted at simulated temperature, pressure and airspeed conditions, that is, full scale Reynolds number. The aerodynamic tests on CADT were conducted at the Wright Brothers Low Speed Wind tunnel at MIT. This tunnel was selected for its capabilities of generating low speed and low turbulence flows. The results of the test are available in full detail (Durgin and Fanucci¹²) with a synopsis presented below.

The wind tunnel operates only at atmospheric pressure and temperature. The stratospheric corona sensor was not designed to operate at pressures above 120 mm Hg since the high voltage was limited to 2000 V. Consequently, it was necessary to use the commercial Thermal Systems Inc. (TSI) anemometer in the wind tunnel tests. The electronics are different between the AFGL and TSI instruments, and the separation gap was a half inch for TSI and one inch for the AFGL instrument. Both instruments used the same collector and anode plates. It was believed that differences were not important for an investigation of the aerodynamic effects and the possibility of instrumental induced turbulence. The Wright Brothers Wind tunnel at the Massachusetts Institute of Technology was operated at atmospheric pressure at speeds from 0.5 m/sec to 14 m/sec with controlled amounts turbulence. Turbulent flows were generated by installing a wooden grid at the beginning of the test section. The grid, constructed of a square lattice of 1 in. \times 3 in. boards spaced

12. Durgin, F. H., and Fanucci, J. P. (1977) Static and Dynamic Calibration of a Corona Discharge Anemometer, AFGL-TR-77-0022.

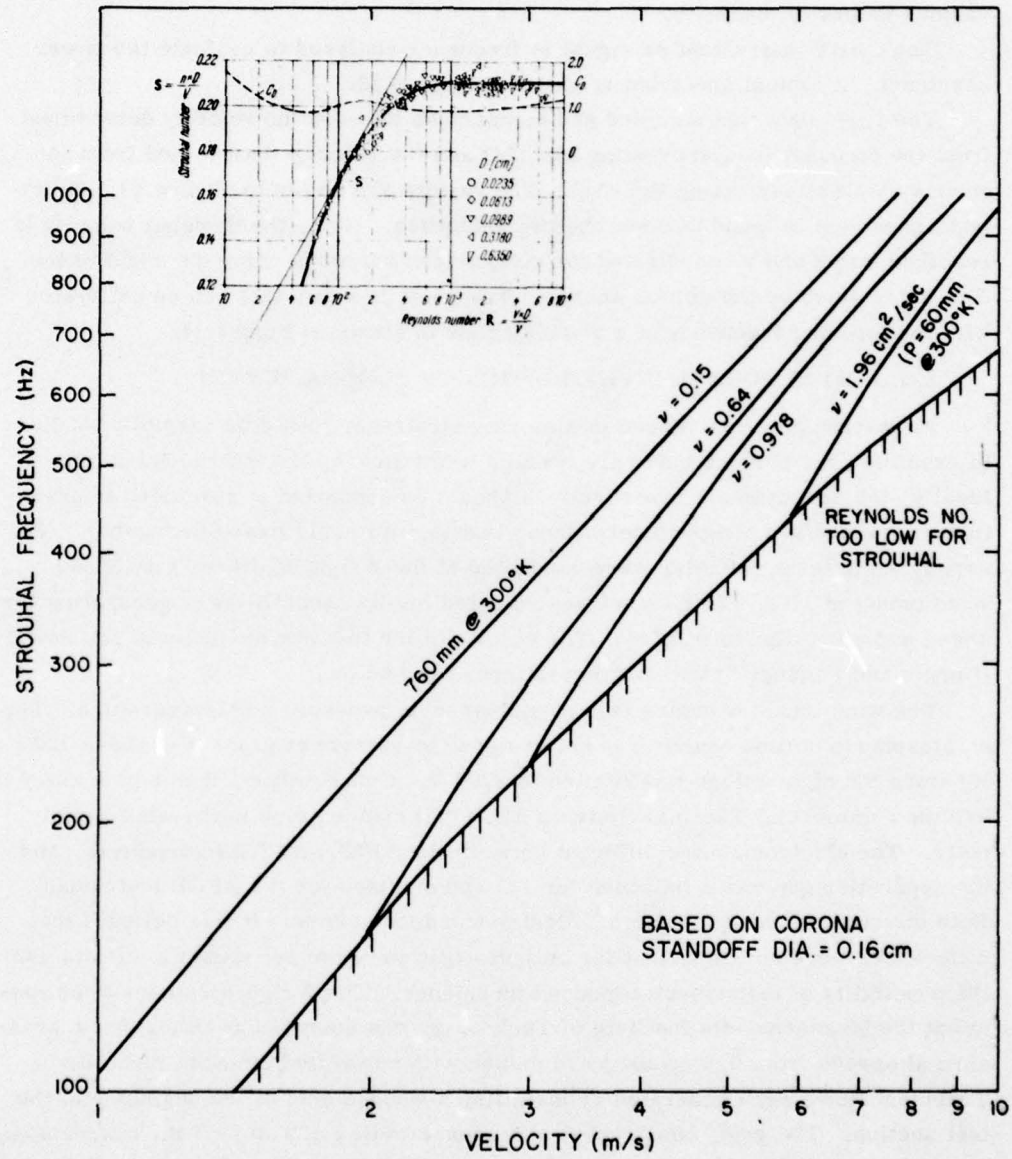


Figure 11. Strouhal Velocity Calibration

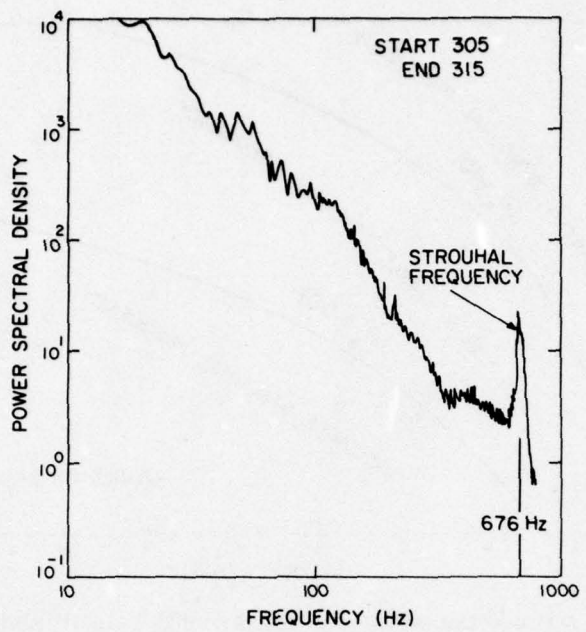


Figure 12. Power Spectral Density of Corona Anemometer Voltage Showing the Strouhal Frequency

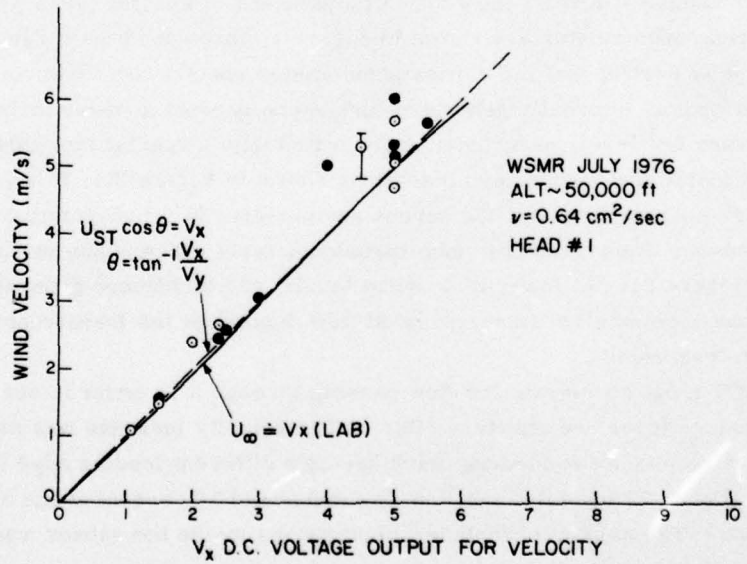


Figure 13. Comparison of Bell Jar Velocity Calibration With In-flight Calibration Using Strouhal Velocity Calibration

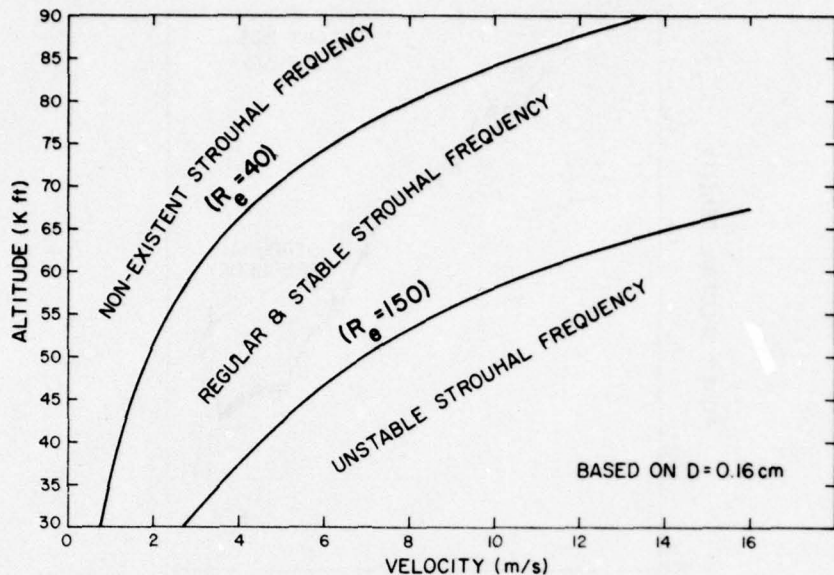


Figure 14. Altitude Domain Useful for Strouhal Velocity Calibration

12 in. apart (see Figure 15) was designed using data from Baines and Peterson¹³ to produce a flow which varied from 20 percent turbulence, 2 m from the grid to 5 percent turbulence 4 m from the grid. Comparisons of spectra taken with a hot wire and corona anemometer are shown in Figure 16 through 19 for a range of flow velocities. It is evident that the corona anemometer spectra are identical to hot wire spectra with no internally generated turbulence present at these turbulence levels. At very low levels of turbulence generated with a special fan, turbulence is generated inside the corona anemometer as shown in Figure 20. It is apparent that the power spectra from the TSI corona anemometer is representative of free-stream turbulence when the freestream turbulence level exceeds one percent. This is shown in Figure 21. At lower turbulence levels, the turbulence generated inside the TSI corona anemometer from separated flow dominates the freestream turbulence at high frequencies.

The CADT must accelerate the flow passing through it in order to accommodate the boundary layer and aperture effect. The velocity increase was measured with the hot wire inside two models, each having a different leading edge radius of curvature. Figure 22 indicates the flow is accelerated 10 percent at the center of corona sensor. The amount of turbulent fluctuations inside the sensor was also

13. Baines, W. D., and Peterson, E. G. (1951) An investigation of flow through screens, Trans. ASME, pp 467-480.

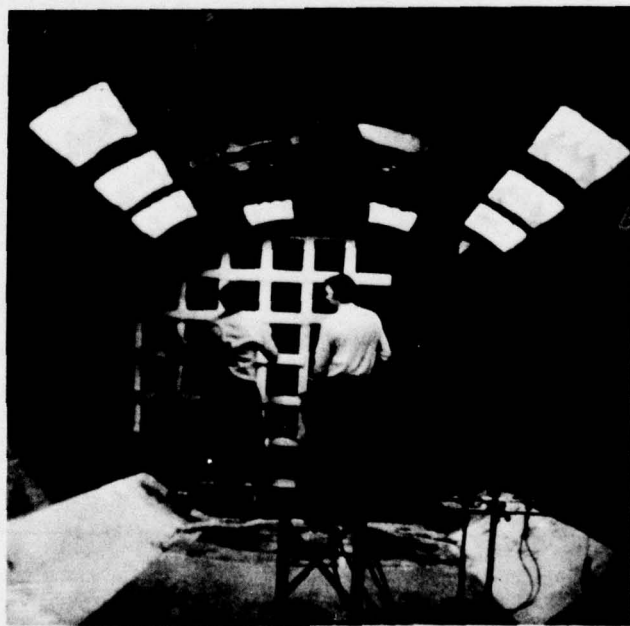


Figure 15. Wind Tunnel Calibration of Corona Anemometer

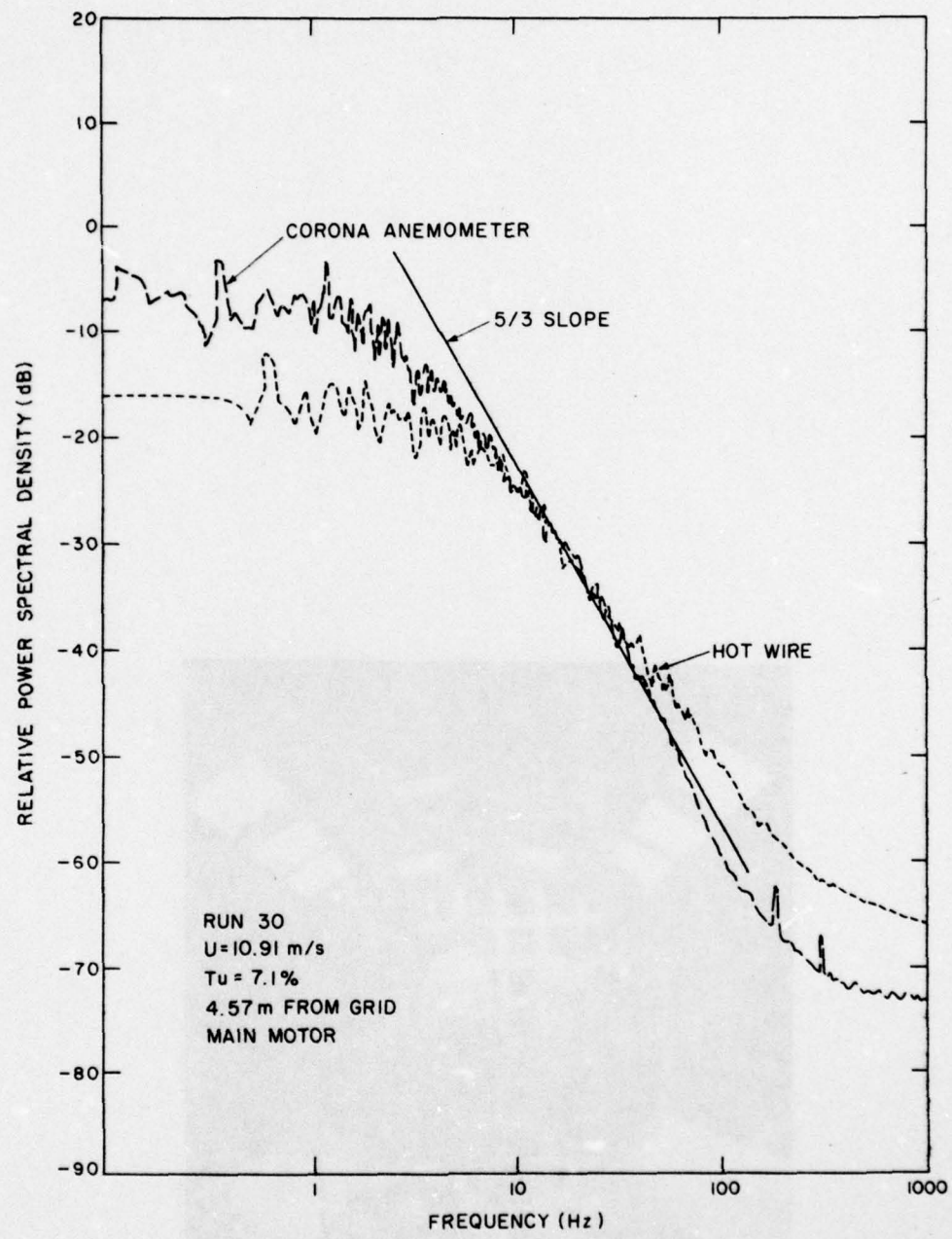


Figure 16. Power Spectral Density Comparison of Hot Wire and Corona Anemometer, $U = 10.91 \text{ m/sec}$, $X = 4.57 \text{ m}$

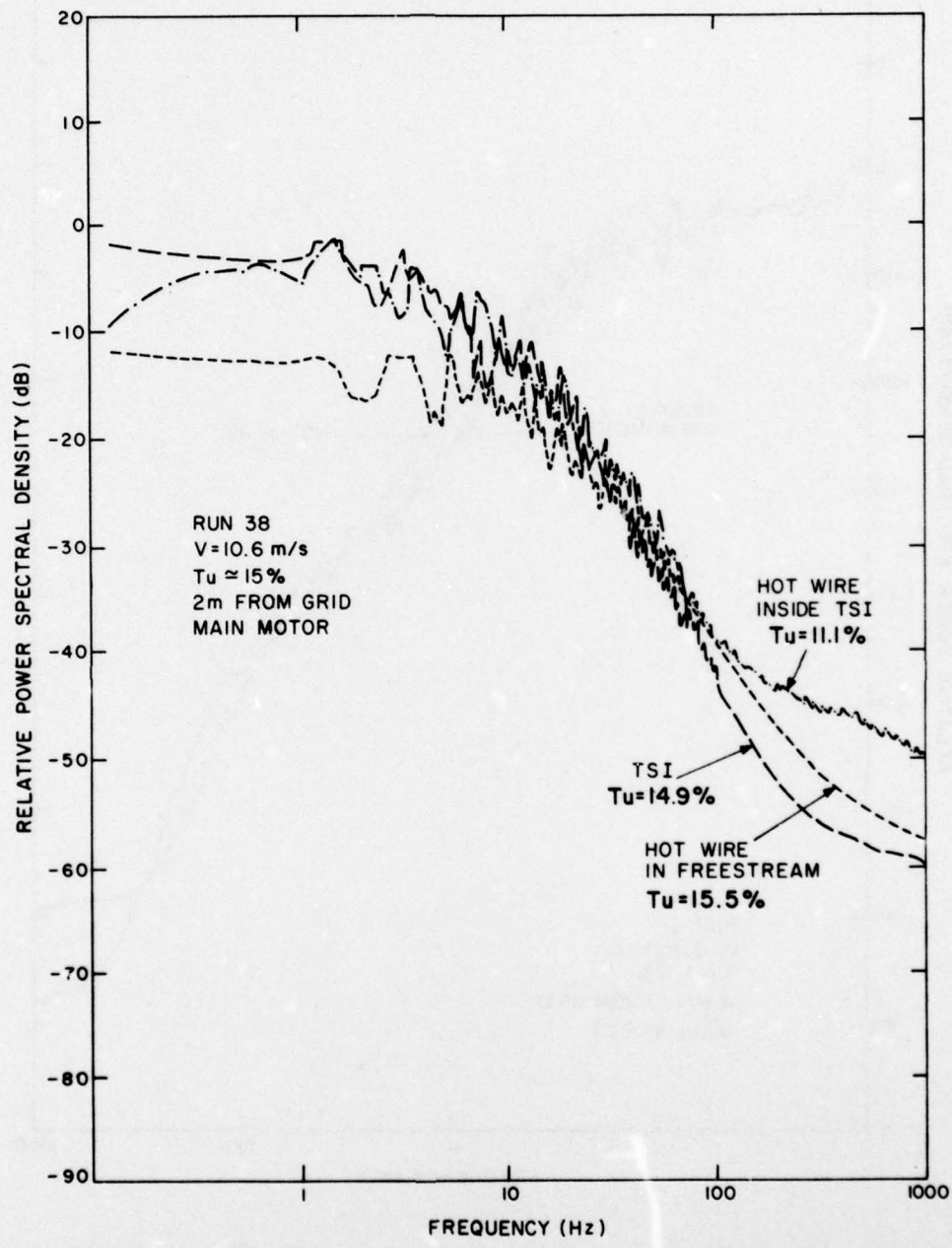


Figure 17. Power Spectral Density Comparison of Hot Wire and Corona Anemometer, $U = 10.6 \text{ m/sec}$, $X = 2\text{m}$

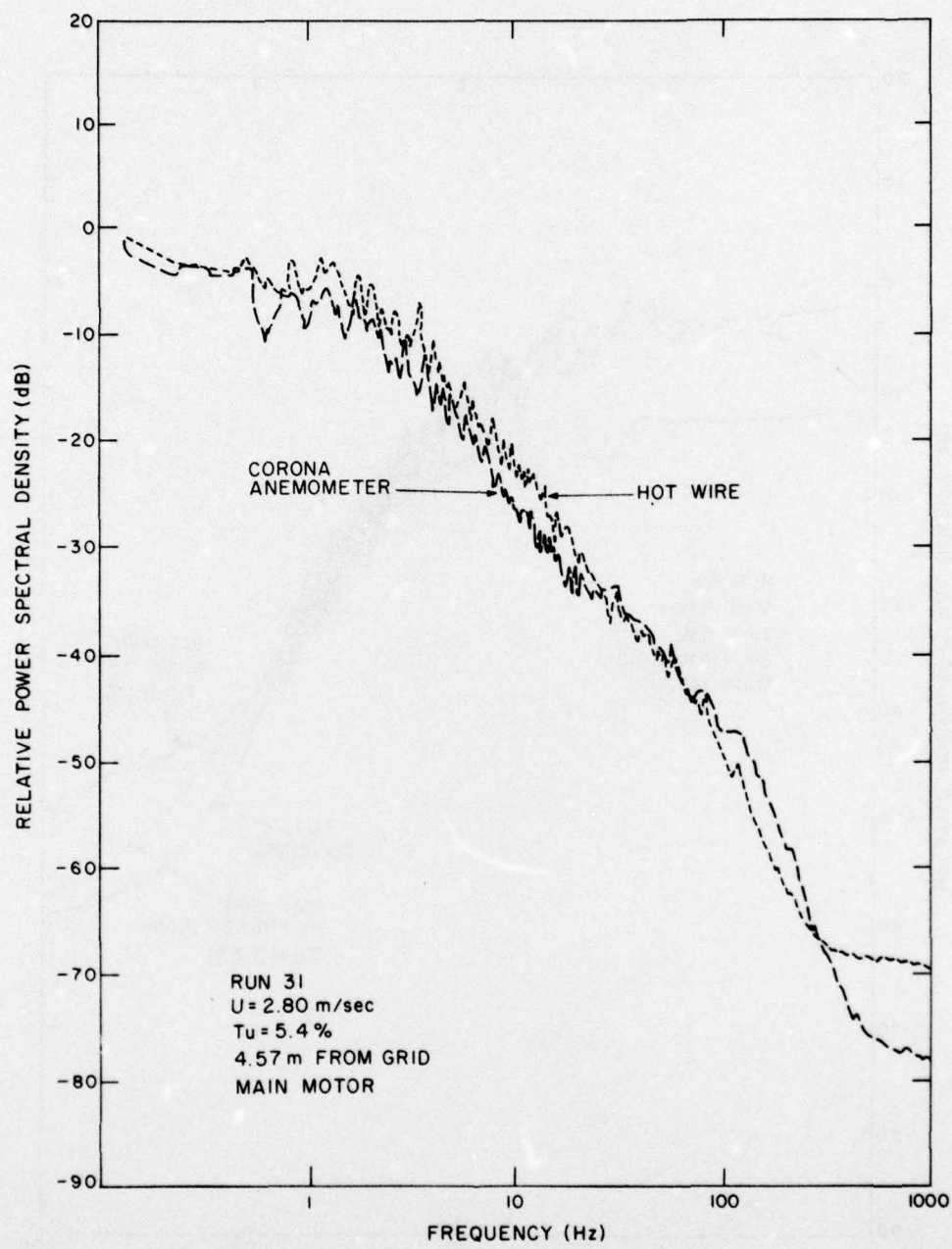


Figure 18. Power Spectral Density Comparison of Hot Wire and Corona Anemometer, $U = 2.8$ m/sec, $X = 4.57$

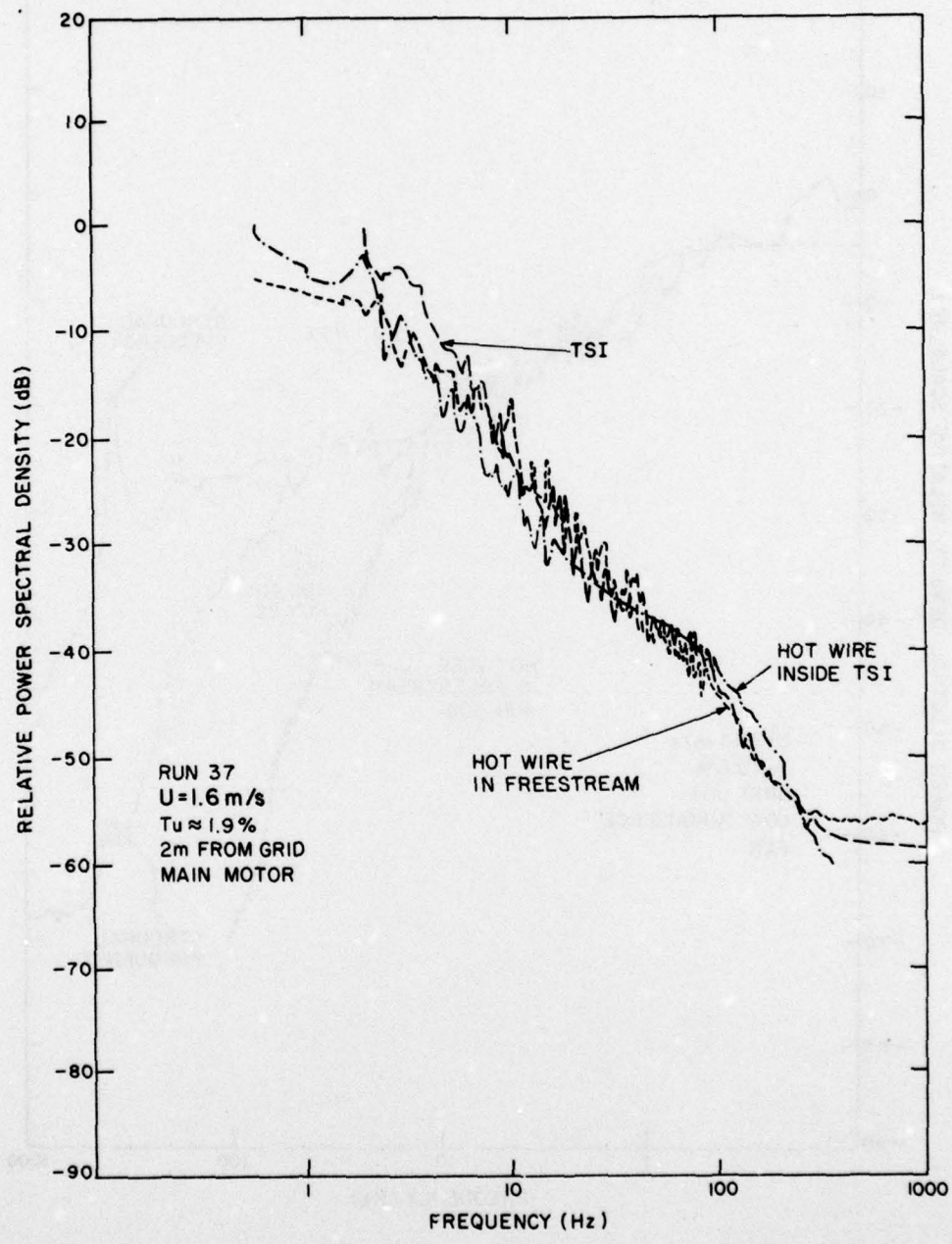


Figure 19. Power Spectral Density Comparison of Hot Wire and Corona Anemometer, $U = 1.6 \text{ m/sec}$, $X = 4.57$

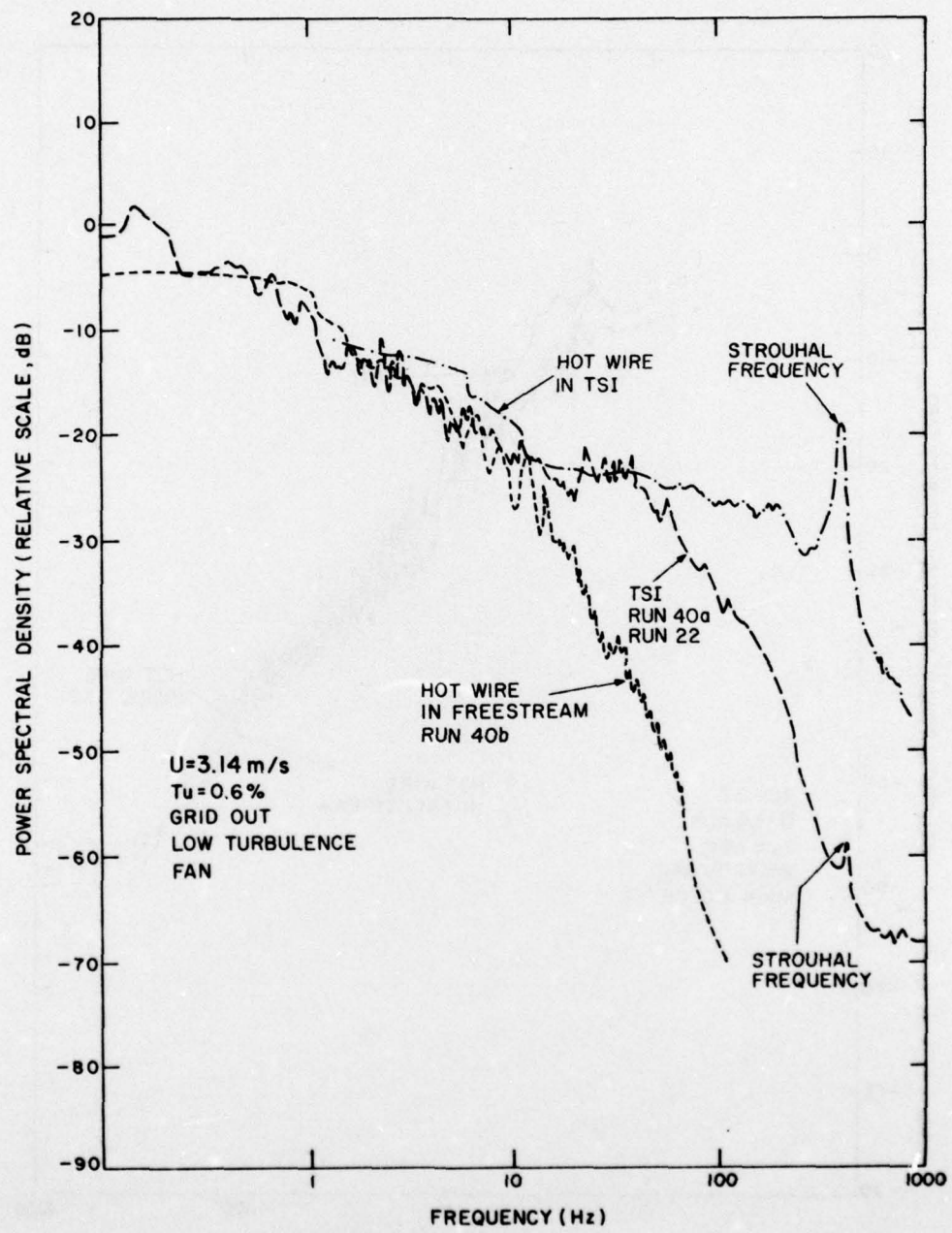


Figure 20. Power Spectral Density Comparison of Hot Wire and Corona Anemometer, $U = 3.14$ m/sec, Grid Out

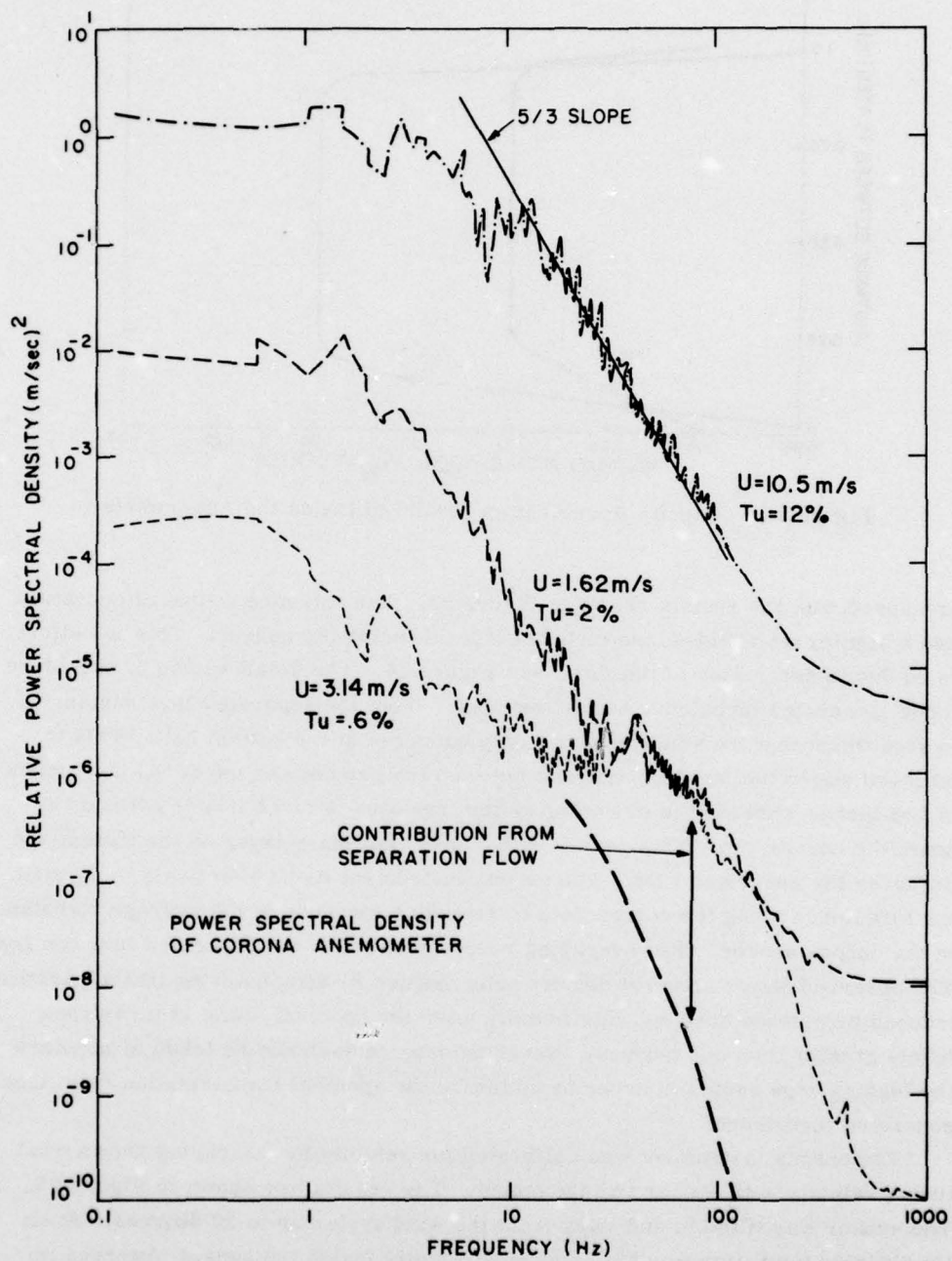


Figure 21. Summary of Power Spectral Density Distributions With Varying Levels of Turbulence

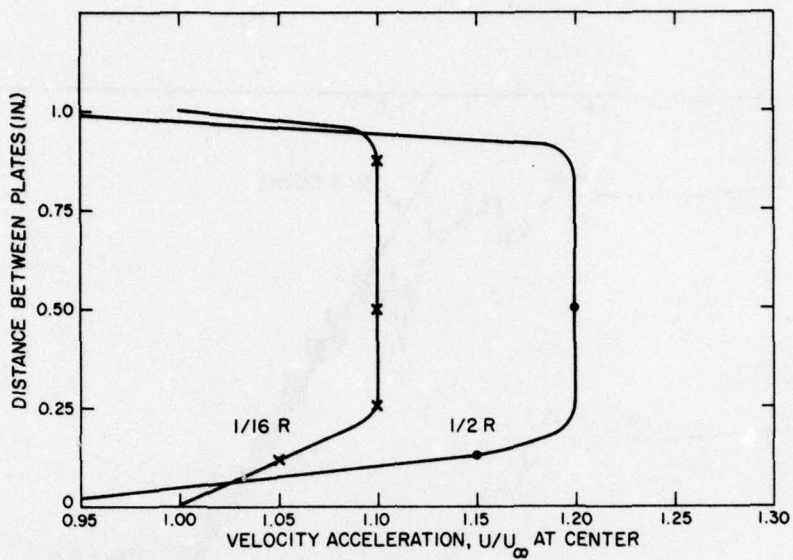


Figure 22. Velocity Acceleration Produced Inside the Anemometer

measured with the results shown in Figure 23. The entrance radius of curvature has a significant effect on the turbulence level inside the sensor. This is believed to be due to separation of the flow, see Figure 24. The small radius of curvature model generates turbulence inside the sensor from the separated flow region. It is significant that the separated flow only occurred at the bottom half. This is believed due to the fact that distance between the gap and the top of the instrument is two inches whereas the mounting system resulted in much longer cylinder beneath the corona gap. This results in a thicker boundary layer on the bottom and produces the separated flow. The corona instrument itself effectively integrates the turbulence along the corona path to provide a measure of the average turbulence in the corona sensor. The averaging reduces the effect the separated flow can have. The observed power spectral density data, Figure 21 demonstrates that separation induced turbulence does not significantly alter the spectral shape at turbulence levels greater than one percent. Nevertheless, care should be taken to increase the leading edge radius in order to minimize the spectral contamination from locally generated turbulence.

The corona instrument was calibrated for velocity by comparing known wind tunnel velocity with sensor voltage output. The results are shown in Figure 25. The sensor was tilted in and away from the wind vector up to 30 degrees. At no time during the tilting was the measured velocity inside the sensor observed to change.

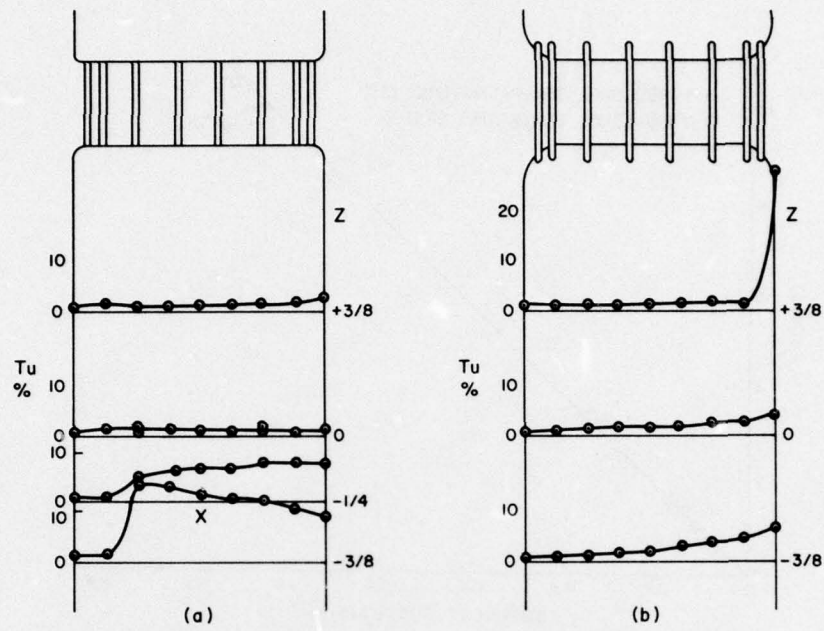


Figure 23. Turbulent Intensity Distribution Inside the First and Second Models of Corona Anemometer

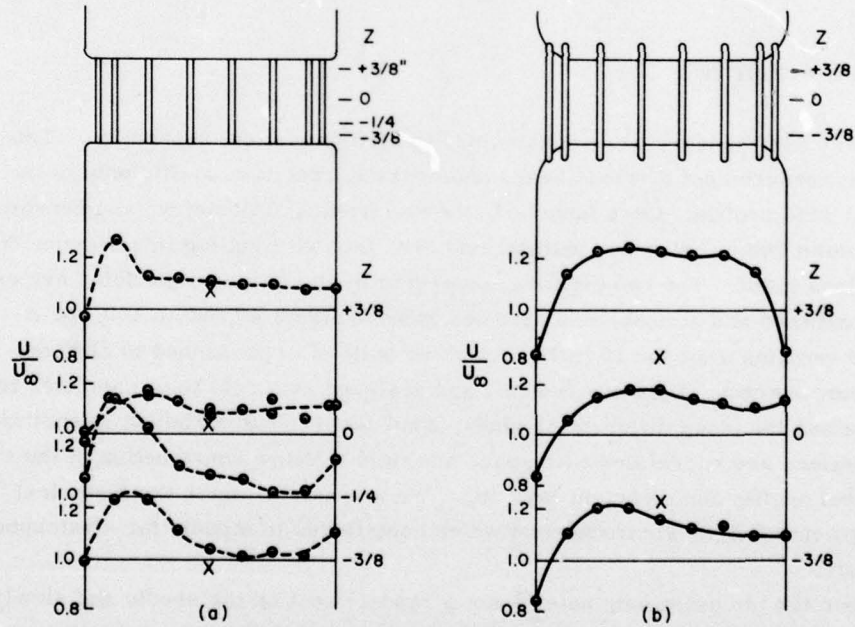


Figure 24. Velocity Distribution Inside the First and Second Models of Corona Anemometer

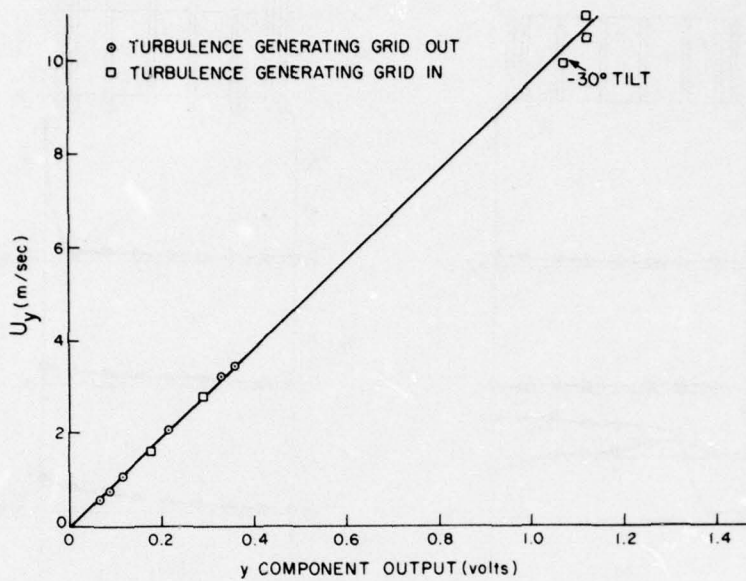


Figure 25. Wind Tunnel Calibration of Velocity Including Effects of Angle of Attack

3. INITIAL FLIGHT TEST

Two CADT sensors were constrained to a 10 m vertical separation. This allowed measurement of wind shears and cross-correlation coefficients of the vertical wind profile. Once launched, the electronics, telemetry, and sensors are reeled down 200 m below the balloon load bar, thus eliminating interference from the balloon itself. The two sensors, protected in an aluminum gondola, are extended outward and atmospheric data are gathered from 40,000 to 100,000 ft. The payload remains aloft for 10 to 12 hr and the balloon is positioned to altitudes of maximum interest. Data are reduced and analyzed by a real time computer to yield values for mean differential winds, wind shears, and turbulent intensities. These values are correlated with space and time to allow construction of the vertical wind profile and turbulent layering. We are able to watch the historical development of clear air turbulence which contributes to models for stratospheric transport.

Since the ion beam originates from a random spot on the needle and slowly travels about the needle, the zero-wind position of the ion beam centerline as it falls on the target plate must be determined. This is done by periodically closing

a shutter over the airstream gap. The sensor automatically measures the zero-wind offset currents and corrects it to zero.

Upon completion of the experiment, the sensors are reeled back into their protective shrouds. The payload is cut from the loadbar and descends on its own parachute to a site where a recovery crew is standing by.

The initial flight was conducted from Holloman AFB on 28 July 1976 at 4 AM. The corona instrument was turned on at 15.1 km with measurement of stratospheric wind shear and turbulence conducted up to 15.8 km. The experiment was terminated after 10 min. of data due to loss of power resulting from damage to the instrumentation package and one sensor during launching of the balloon payload. The altitude excursion measured in this brief flight is shown in Figure 26. The measured pressure, temperature, and velocity sensed by the corona instrument is shown in Figure 27. The velocity measured represents the velocity difference between the balloon and the corona anemometer. The anemometer was reeled down 296 m from the balloon to avoid balloon wake effects. It is assumed that the 172 ft diameter balloon drifts with the wind.

The temperature minimum occurred at 15.45 km. Thus, this first flight yields a measurement above and below the tropopause. The turbulent intensity of this region as determined from the variance of the velocity is shown in Figure 28. A large turbulent layer is located just below the tropopause. Spectral power density distributions were computed from the measured velocity and are shown in Figure 29. The data show the flight instrument has a noise power spectrum distribution with a $-5/3$ slope with frequency. The first spectra shown for time 0 exhibits the same $-5/3$ slope. As the balloon rises and passes through the large turbulent, layer, the sequence of power density spectral indicates a rise and then decay in spectral energy near 200 Hz. An interesting feature is the -6 slope of the spectral energy that exists when the corona is in the turbulent layer. An altitude profile of turbulent dissipation rate is given in Figure 30. This curve is very similar to the velocity variance, as should be expected.

The results contained in this report are given to illustrate the operational capability of the corona anemometer. A thorough evaluation of the measurements, including analysis of the rate of turbulent dissipation, evaluating of turbulent scale lengths and characterization of the turbulent layers will be presented in another technical report.

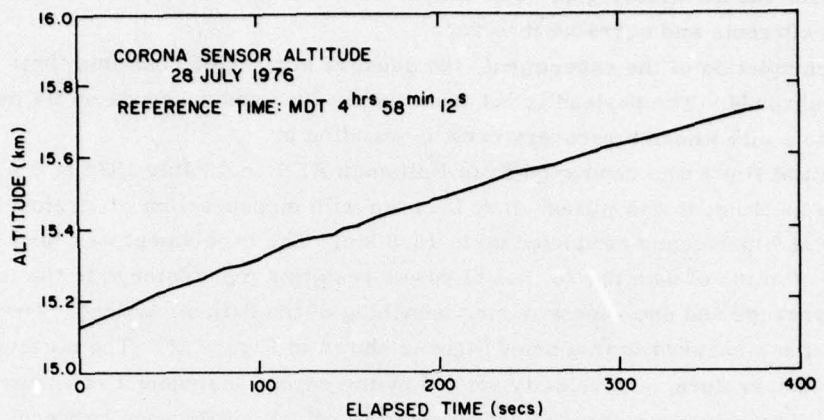


Figure 26. Altitude Profile of Initial Flight Test of Corona Anemometer

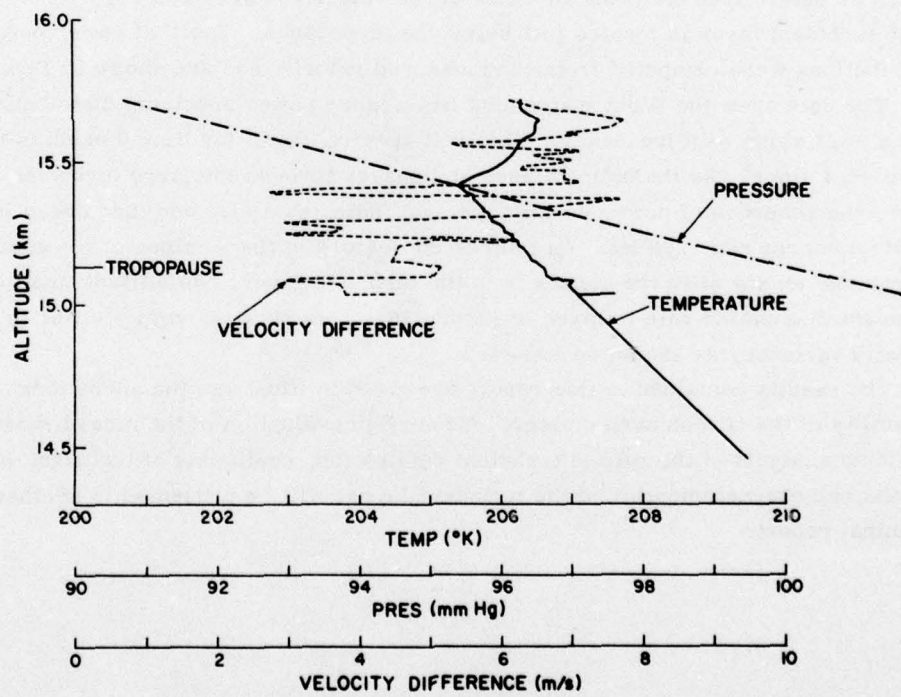


Figure 27. Observed Atmospheric Pressure and Temperature and the Velocity Measured by the Corona Anemometer

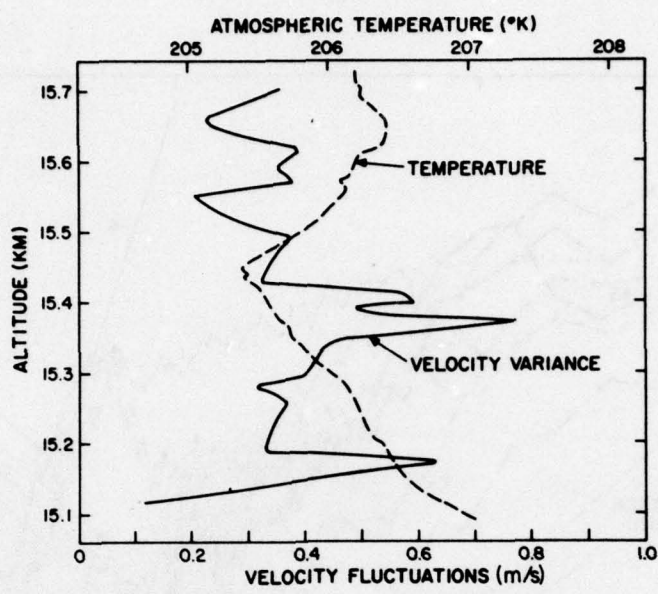


Figure 28. Velocity Variance Observed During Flight

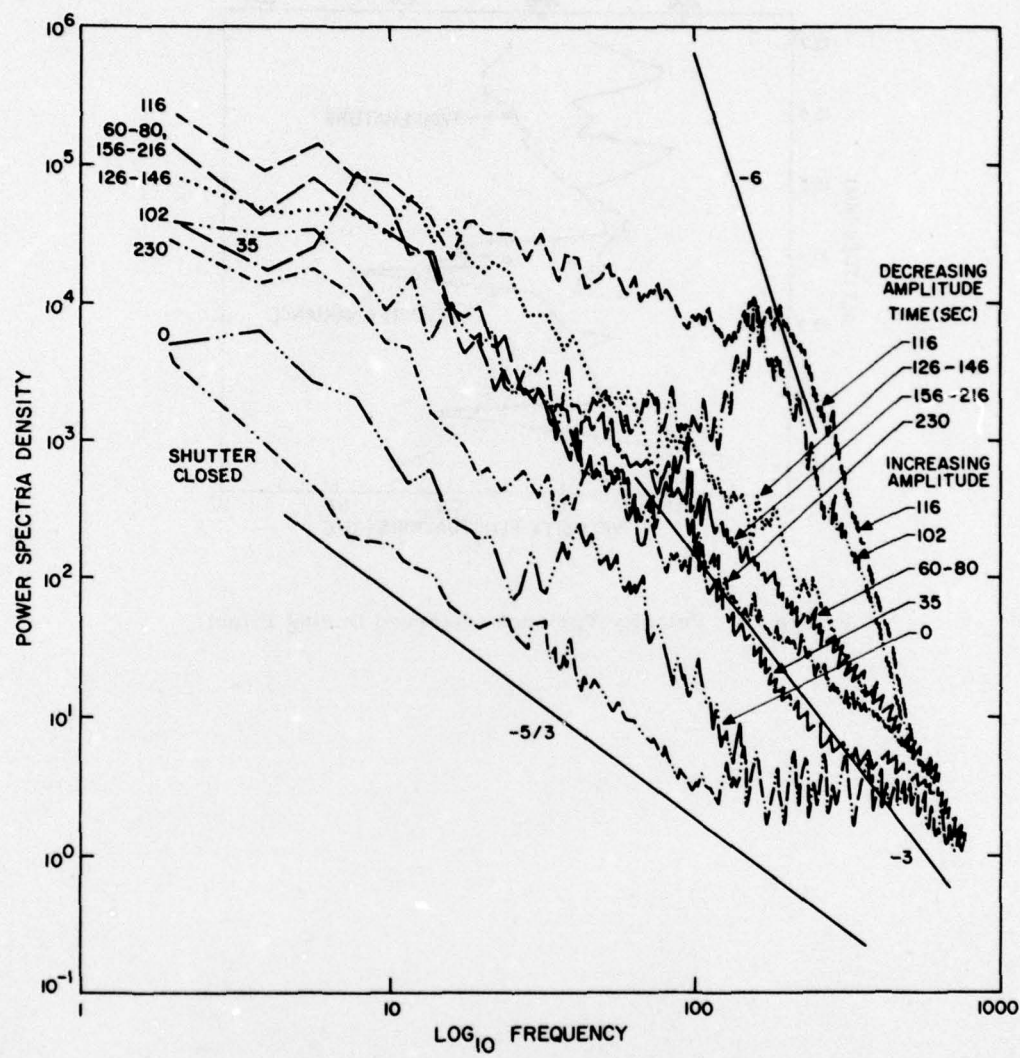


Figure 29. Change of Power Spectral Density as Corona Instrument Passes Across a Turbulent Layer

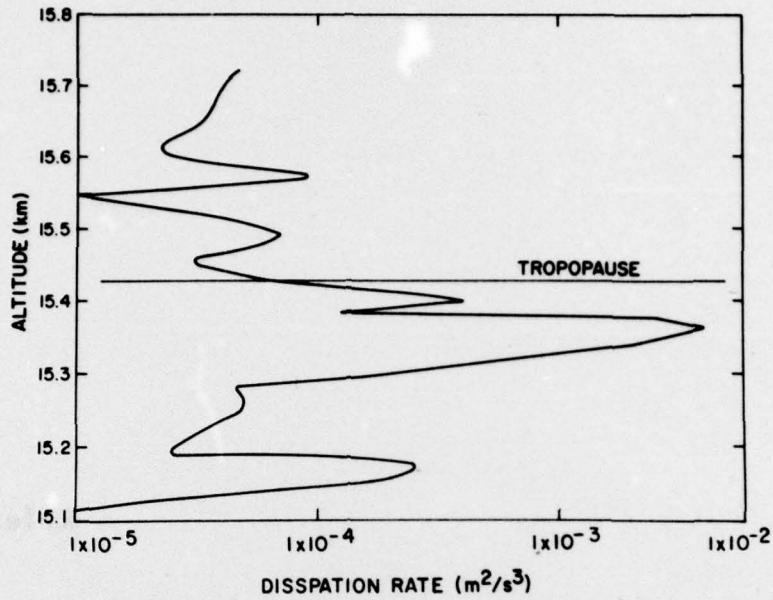


Figure 30. Altitude Profile of Turbulent Dissipate Rate

4. CONCLUSIONS

A new wind and turbulence sensor capable of operating in the stratosphere has been designed, calibrated and flight tested. The sensor, utilizing the principle of a corona ion beam deflected by the airstream, is shown to function properly and measure turbulent wind velocities out to a frequency of 2000 Hz. The corona sensor data can be analyzed to directly determine the turbulent energy contained in the thin turbulence present in the stratosphere. Two sensors, separated some 10 m can be flown to directly measure the vertical gradient of the horizontal wind velocity and the temperature gradient. This permits a direct evaluation of the Richardson number, a parameter related to the occurrence of turbulent layers in the stratosphere. Future flights are planned to obtain altitude profiles of the turbulence layers and the time history of given turbulent layers. The latter can be obtained by positioning the balloon to float in a turbulent layer.

As of 28 April 1978, six individual flights have taken place from Holloman AFB, NM. Refined methods of calibration and analysis have been developed. Also a new ion time-of-flight instrument has been developed which can make in-situ measurements of the DC winds. These developments will appear in another report.

References

1. Franzen, B., Fucks, W., and Schmitz, G. (1961) Corona anemometer for measurement of turbulence components, Zeit. für Flugwissenschaften 9:347-351.
2. Barat, J. (1975) Une méthode de mesure directe du taux de dissipation d'énergie turbulente dans la stratosphère. Compt. Rend. Acad. Sci. Paris B281: 53-56.
3. Lilienfeld, Pedro, Solon, L., and DiGiovanni, Hugo (1967) Ion tracer anemometer for the measurement of low density flows. Rev. Sci. Inst. 38:405-409.
4. Loeb, L. B. (1960) Basic Processes of Gaseous Electronics, Univ. of California Press, Los Angeles.
5. Loeb, L. B. (1965) Electrical Coronas, Univ. of California Press, Los Angeles.
6. Brown, S. C. (1966) Introduction to Electrical Discharges in Gases, John Wiley & Sons, New York.
7. McDaniel, E. W., and Mason, E. A. (1973) The Mobility and Diffusion of Ions in Gases, John Wiley & Sons, New York.
8. Waletzko, J. A. (1975) A new ion displacement system to measure the two dimensional wind vector, Tech. Conf. on Automated Meteorological Systems, Washington, D. C.
9. Roshko, R. (1954) On the Development of Turbulent Wakes From Vortex Streets, NACA Rep 1191.
10. Webster, C. A. G. (1964) An experimental study of turbulence in a density-stratified shear flow, Fluid Mech. 19:221-245.
11. Tritton, D. J. (1970) Experiments on the Flow Past a Circular Cylinder at Low Reynolds Numbers.
12. Durgin, F. H., and Fanucci, J. P. (1977) Static and Dynamic Calibration of a Corona Discharge Anemometer, AFGL-TR-77-0022.
13. Baines, W. D., and Peterson, E. G. (1951) An investigation of flow through screens, Trans. ASME, pp 467-480.